Published in final edited form as:

Nature. 2020 August ; 584(7820): 291–297. doi:10.1038/s41586-020-2545-9.

Lysosome-targeting chimaeras for degradation of extracellular proteins

Steven M. Banik[1], **Kayvon Pedram**[1], **Simon Wisnovsky**[1], **Green Ahn**[1], **Nicholas M. Riley**[1], **Carolyn R. Bertozzi**[1,2,✉]

[1]Department of Chemistry, Stanford University, Stanford, CA, USA.

[2]Howard Hughes Medical Institute, Stanford, CA, USA.

Abstract

The majority of therapies that target individual proteins rely on specific activitymodulating interactions with the target protein–for example, enzyme inhibition or ligand blocking. However, several major classes of therapeutically relevant proteins have unknown or inaccessible activity profiles and so cannot be targeted by such strategies. Protein-degradation platforms such as proteolysis-targeting chimaeras (PROTACs)[1,2] and others (for example, dTAGs[3], Trim-Away[4], chaperone-mediated autophagy targeting[5] and SNIPERs[6]) have been developed for proteins that are typically difficult to target; however, these methods involve the manipulation of intracellular protein degradation machinery and are therefore fundamentally limited to proteins that contain cytosolic domains to which ligands can bind and recruit the requisite cellular components. Extracellular and membrane-associated proteins—the products of 40% of all protein-encoding genes[7]–are key agents in cancer, ageing-related diseases and autoimmune disorders[8], and so a general strategy to selectively degrade these proteins has the potential to improve human health. Here we establish the targeted degradation of extracellular and membrane-associated proteins using conjugates that bind both a cell-surface lysosome-shuttling receptor and the extracellular domain of a target protein. These initial lysosome-targeting chimaeras, which we term LYTACs, consist of a small molecule or antibody fused to chemically synthesized glycopeptide ligands that are agonists of the cation-independent mannose-6-phosphate receptor (CI-M6PR). We use LYTACs to develop a CRISPR interference screen that reveals the biochemical pathway for CI-M6PR-mediated cargo internalization in cell lines, and uncover the exocyst complex as a previously unidentified–but essential–component of this pathway. We demonstrate the scope of this platform through the degradation of therapeutically relevant proteins, including apolipoprotein

✉**Correspondence and requests for materials** should be addressed to C.R.B. bertozzi@stanford.edu.

Author contributions S.M.B., K.P. and C.R.B. conceived the project. S.M.B., K.P., S.W., G.A. and N.M.R. carried out experiments and interpreted data. S.M.B. and C.R.B. wrote the manuscript with input from all authors. C.R.B. provided supervision.

Competing interests C.R.B. is a co-founder and scientific advisory board member of Lycia Therapeutics, Palleon Pharmaceuticals, Enable Bioscience, Redwood Biosciences (a subsidiary of Catalent) and InterVenn Biosciences, and a member of the board of directors of Eli Lilly & Company. S.M.B. is a consultant for Lycia Therapeutics. Stanford University has filed patent applications related to this work which are licensed to Lycia Therapeutics, listing S.M.B., K.P., G.A. and C.R.B. as inventors.

Supplementary information is available for this paper at https://doi.org/10.1038/s41586-020-2545-9.

Peer review information *Nature* thanks Nathanael Gray and the other, anonymous, reviewer(s) for their contribution to the peer review of this work.

E4, epidermal growth factor receptor, CD71 and programmed death-ligand 1. Our results establish a modular strategy for directing secreted and membrane proteins for lysosomal degradation, with broad implications for biochemical research and for therapeutics.

Unlike the proteasomal pathway, the lysosomal pathway for protein degradation is not limited to proteins that have intracellular domains. Families of cell-surface lysosome-targeting receptors (LTRs) have been reported that facilitate the transport of proteins to lysosomes[9]. We proposed that chimeric molecules capable of binding both a cell-surface LTR and an extracellular protein might induce internalization and lysosomal degradation of the target, offering a means to accelerate the degradation of proteins by using binders that act in the extracellular space. The prototypical LTR is the cation-independent mannose-6-phosphate receptor (CI-M6PR, also called IGF2R), which endogenously transports proteins bearing N-glycans capped with mannose-6-phosphate (M6P) residues to lysosomes[10]. The receptor cycles constitutively between endosomes, the cell surface and the Golgi complex. CI-M6PR shuttles cargo efficiently to prelysosomal compartments, where a lowered pH enables cargo to dissociate and progress to the lysosome while CI-M6PR is recycled. On the basis of its ability to efficiently deliver proteins to lysosomes and its expression in a range of different tissue types, CI-M6PR has been exploited to deliver therapeutic enzymes for the treatment of lysosomal storage disorders[11]. Here we present lysosome-targeting chimaeras–which we term LYTACs (Fig. 1a)–that enable the depletion of secreted and membrane-associated proteins via a mechanism of action that is orthogonal and complementary to that of existing technologies[12], and which does not rely on an extracellular protease for efficacy[13]. We show that LYTACs can serve as biochemical probes for the study of receptor trafficking and protein degradation, and can mediate the degradation of both secreted and membrane-associated proteins of therapeutic interest.

To develop ligands for CI-M6PR, we leveraged precedents aimed at enhancing lysosomal enzyme replacement therapies and drug delivery platforms. This previous work included biosynthetic engineering of M6P-bearing glycans[14] as well as chemical synthesis of oligomeric M6P-containing scaffolds[15]. A recurring design parameter from these studies was the requirement for a multivalent ligand, in order to achieve optimal CI-M6PR agonism[16-18]. Previous work had also revealed that the 6-phosphoester could undergo hydrolysis in human serum[19], leading to rapid endocytosis by macrophages bearing mannose receptors[20]. We reasoned that *N*-carboxyanhydride (NCA)-derived glycopolypeptides[21] bearing multiple serine-*O*-mannose-6-phosphonate (M6Pn) residues[22] would enable multivalent presentation on a biocompatible, phosphatase-inert[23] and modular scaffold. We synthesized M6Pn glycopolypeptides starting with the conversion of mannose pentaacetate to M6Pn-NCA in 13 steps (Fig. 1b, Extended Data Fig. 1a). Subsequent copolymerization of M6Pn-NCA and alanine-NCA (1:1 ratio, for the purpose of spacing and polymerization kinetics) provided access to M6Pn glycopolypeptides (post-deprotection dispersity, $Đ = 1.3–1.5$) of various lengths, including short (20 M6Pn) and long (90 M6Pn) variants, to test in protein degradation assays. We also synthesized the corresponding M6P-containing copolymers bearing the natural phosphorylated glycan structure (Extended Data Fig. 1b), with similar molecular weights and dispersities to those obtained with M6Pn monomers.

To demonstrate the feasibility of CI-M6PR-driven LYTACs, we designed an in cellulo assay to measure the uptake of NeutrAvidin-647 (NA-647), an Alexa Fluor-647 (AF647)-labelled protein to which biotin binds (Fig. 1c). We synthesized and biotinylated poly(M6P) and poly(M6Pn) polypeptides, as well as poly(*N*-acetylgalactosamine) (poly(GalNAc)) and poly(mannose) as controls (Fig. 1d, Extended Data Figs. 1c, d, 2a). K562 cells were incubated with either NA-647 or NA-647 and biotinylated glycopolypeptide for one hour, then washed and analysed by flow cytometry. Co-incubation with M6P and M6Pn polypeptides increased cellular fluorescence by 5–6-fold compared with the background, with only minor differences in uptake efficiency observed as a result of glycopolypeptide length (short versus long, Fig. 1e). M6Pn polypeptides showed performance that was equivalent or superior to that of M6P polypeptides of similar length, whereas incubation with mannose- or GalNAc-containing glycopolypeptides showed no marked change in fluorescence compared with the background. NA-647 uptake mediated by poly(M6Pn) was attenuated by co-incubation with excess exogenous M6P. Furthermore, uptake remained continuous over time (Extended Data Fig. 2b), suggesting that surface-receptor recycling was the rate-limiting step[24]. AF647 is reported to be stable in endosomes and lysosomes[25], with a steadily increasing fluorescent signal arising from intracellular fluorophore accumulation. Live-cell fluorescence microscopy experiments revealed that the AF647 signal co-localized with acidic endosomes and lysosomes after only 1 h (Fig. 1f, Extended Data Figs. 2c, d). Finally, biotinylated LYTACs mediated NA-647 uptake in various cell lines, demonstrating the breadth of CI-M6PR-targeting (Fig. 1g) as well as the ability to use small molecules as LYTAC ‘warheads’.

We next performed a CRISPR interference (CRISPRi) pooled genetic screen with the aim of identifying genes for which knockdown ablates the delivery of NA-647 by biotinylated LYTACs[26,27] (Fig. 2a). K562 cells expressing dCas9-KRAB were transduced with a genome-wide library of CRISPRi single guide RNAs (sgRNAs) and incubated with LYTAC and NA-647. A population of cells that exhibited a substantial decrease in NA-647 labelling was isolated by fluorescence-activated cell sorting (FACS), and next-generation sequencing was performed to identify sgRNAs that were overrepresented in this population. Guide RNAs to *IGF2R* (which encodes CI-M6PR) were highly enriched in the sorted pool, providing unbiased confirmation of selective receptor targeting (Fig. 2b; for the full dataset, see Supplementary Information). Other significantly enriched guide RNAs (false discovery rate (FDR) < 5%) targeted genes that regulate endosomal acidification, vesicle trafficking, endosome–lysosome fusion and clathrin-dependent endocytosis (Fig. 2c), consistent with a CI-M6PR-driven endocytic pathway to lysosomes[10]. Components of the exocyst complex–which is reported to mediate vesicle localization to the plasma membrane[28]–were also identified as essential for the M6Pn-mediated internalization of NA-647. We proposed that the exocyst complex could be involved in the presentation of CI-M6PR on the cell surface, a biochemical pathway which is yet to be elucidated[10]. We performed CRISPRi knockdown of *EXOC1* and *EXOC2* (which encode the exocyst complex components 1 and 2, respectively) in K562 cells using CRISPRi library guides, and measured cell-surface CI-M6PR levels by flow cytometry. A 60% decrease in cell-surface CI-M6PR levels was observed (Fig. 2d). We replicated these results in HeLa cells (75% decrease, Fig. 2e), and found that total CI-M6PR levels did not change upon knockdown of *EXOC1* in either cell line (Fig. 2f, g,

respectively). Further, we observed no change in surface expression of epidermal growth factor receptor (EGFR) on HeLa cells (Extended Data Fig. 3), indicating that the global trafficking of cell-surface proteins remained unperturbed. Together these data indicate that the surface presentation of CI-M6PR is mediated in part by the exocyst complex, and–more broadly–that LYTACs can be used to study the molecular pathways involved in the regulation of cell-surface receptors.

We next sought to determine whether conjugation of a poly(M6Pn)-bearing glycopolypeptide to an antibody would reprogramme the antibody to rapidly direct extracellular agents to the lysosome. As a proof-of-principle experiment, we non-specifically labelled lysine residues on a polyclonal anti-mouse IgG with bicyclononyne-*N*-hydroxysuccinimide (BCN-NHS), and subsequently conjugated this antibody to azide-terminated M6Pn glycopolypeptides via copper-free strain-promoted azide–alkyne cycloaddition (Fig. 3a), generating the LYTAC **Ab-1**. The conjugation reaction could be readily monitored by native gel electrophoresis, because the covalent attachment of the anionic polypeptides caused a characteristic enhancement in migration compared with antibodies conjugated with non-charged polypeptides (that is, poly(GalNAc)) (Fig. 3b). Incubation of K562 cells with **Ab-1** and a mouse IgG labelled with Alexa Fluor-488 (AF488) (Extended Data Fig. 4a) resulted in a 40-fold increase in lysosomal AF488 signal relative to that of controls (Extended Data Fig. 4b, c).

Given that **Ab-1** efficiently trafficked IgG molecules to lysosomes, we reasoned that it could function as a LYTAC for a primary IgG antibody bound to its antigen (Fig. 3c). Co-incubation of cells with mCherry, mouse anti-mCherry and **Ab-1** resulted in increases in uptake of between 10-fold and 100-fold relative to non-M6Pn-bearing antibodies in cell lines (Fig. 3d-f). We next aimed to expand this strategy to a clinically relevant target, selecting apolipoprotein E4 (ApoE4), which has been implicated in the pathogenesis of neurodegenerative disease[29]. A 13-fold increase in uptake of ApoE4-647 was observed using **Ab-1** and a mouse anti-ApoE4 primary antibody (Fig. 3g), and uptake was continuous over the course of the incubation (Extended Data Fig. 4d). Co-localization of the AF-647 signal with lysosomes was observed at both 1 h and 24 h (Extended Data Fig. 4g), replicating our findings with NeutrAvidin and IgG. Notably, non-specific inhibition of serine and cysteine proteases resulted in the accumulation of intracellular ApoE4-647, and this accumulation was substantially increased in the presence of anti-ApoE4 with **Ab-1** (Fig. 3h, Extended Data Fig. 4e, f). These data demonstrate that LYTAC-mediated target enrichment in the lysosome is coupled with target degradation. More broadly, conjugation of a lysosome-targeting ligand to an antibody can reprogramme the antibody to direct an extracellular antigen for degradation.

We next asked whether LYTACs could be used to accelerate the degradation of membrane-bound extracellular proteins. In principle, this requires simultaneous binding of a surface-associated protein and engagement of CI-M6PR, an interaction which would also benefit from increased effective molarity upon target binding (Fig. 4a). We first targeted EGFR, a known driver of cancer proliferation that can perform multiple scaffolding functions regardless of inhibition of its receptor tyrosine kinase activity. LYTACs were constructed using cetuximab (ctx)–an EGFR-blocking antibody approved by the Food and Drug

Administration (FDA)–using a similar scheme to **Ab-1** (Extended Data Fig. 5a). HeLa cells were incubated for 24 h with 100 nM ctx, ctx functionalized with either long or short M6Pn glycopolypeptides, or GalNAc-functionalized ctx as a control. Cells were then lysed and assayed for total EGFR levels (Extended Data Fig. 5b). Substantial degradation of EGFR was observed only with ctx conjugates bearing M6Pn glycopolypeptides (greater than 70% degradation, comparable to EGF-induced downregulation), while no changes in CI-M6PR levels were observed. There was no apparent difference in degradation ability between LYTACs bearing short or long M6Pn glycopolypeptides. To demonstrate that depletion of EGFR is mediated by CI-M6PR, we compared the degradation performance of ctx-M6Pn **Ab-2** (Extended Data Fig. 5c) to that of unmodified ctx in dCas9-KRAB HeLa lines stably expressing a non-targeting or an *IGF2R*-targeting sgRNA. Degradation of EGFR was observed only in HeLa cells that expressed non-targeting sgRNA, whereas knockdown of *IGF2R* completely abrogated the degradation mediated by **Ab-2** (Fig. 4b). Equivalent results were obtained with concentrations of **Ab-2** of between 100 nM and 10 nM (Extended Data Fig. 5e). EGFR degradation was observed after 3 h and reached a maximum between 12 h and 24 h, persisting for at least 72 h (Extended Data Fig. 5f, g). Exogenous M6P inhibited the degradation of EGFR (Fig. 4c) in the presence of **Ab-2**, whereas treatment of cells with chloroquine prevented **Ab-2**-promoted degradation, demonstrating a dependency both on M6P binding and on lysosomal acidification. To rule out the possibility that EGFR crosslinking by ctx contributes to target downregulation[30,31], we digested ctx with papain to obtain ctx-Fab–which binds EGFR in a monovalent fashion–and conjugated it to poly(M6Pn) to generate **Fab-1** (Extended Data Fig. 5d). **Fab-1** accelerated the degradation of EGFR, in a CI-M6PR-dependent manner, to levels comparable with those obtained using **Ab-2** (Fig. 4d); this demonstrates that monovalent target binders can be used as LYTACs. In a mixed cell assay with HeLa (CI-M6PR$^+$EGFR$^+$) and Jurkat (CI-M6PR$^+$EGFR$^-$) cells, the ctx–M6Pn conjugate exhibited a similar binding profile to that of ctx alone, suggesting that LYTACs with dual affinities for the target and CI-M6PR can maintain high on-target specificity (Extended Data Fig. 6). EGFR degradation was also observed in breast cancer (BT474 and MDA-MB-361) and hepatocellular carcinoma (Hep3B and HepG2) cell lines (Fig. 4h, Extended Data Fig. 7a).

Next, we used quantitative mass spectrometry to perform a proteome-wide characterization of LYTAC degradation specificity in cells treated with ctx or **Ab-2**. A significant reduction of EGFR levels was promoted by **Ab-2**, whereas ctx did not affect EGFR levels (Fig. 4e). CI-M6PR levels were unchanged, further supporting that the degradation of EGFR is catalytic in terms of CI-M6PR. Changes in the expression levels of other proteins as a result of EGFR degradation were also observed (Extended Data Table 1; for the full dataset, see Supplementary Information). These co-degraded proteins may represent EGFR interaction partners or co-regulated molecules. For example, treatment with **Ab-2** caused significant downregulation of dihydropteridine reductase, 7,8-dihydro-8-oxoguanine triphosphatase and transcription factor DP-1, and resulted in the upregulation of glucose-1,6-bisphosphate synthase and coordinator of PRMT5 and differentiation stimulator (COPRS). Although the precise mechanism for these changes remains to be elucidated, these data suggest that LYTACs may provide a means to monitor cellular changes in response to targeted protein degradation.

We compared the functional consequences of LYTAC-mediated degradation to those of EGFR inhibition by ctx. Immunofluorescent microscopy revealed marked relocalization of EGFR from the plasma membrane to intracellular vesicles upon treatment with **Ab-2** compared to treatment with ctx alone (Fig. 4f). To assess the consequences of degradation and removal from the plasma membrane, we incubated cells with ctx or **Ab-2**, then washed and treated them with EGF. In cells left untreated by ctx or **Ab-2**, we observed rapid phosphorylation of Tyr1068 of EGFR that decreased over time–this is consistent with EGF-induced downregulation of EGFR (Fig. 4g). Cells treated with ctx exhibited modest levels of phosphorylation that were sustained for the course of the EGF incubation. The sustained levels of phosphorylation are consistent with the ability of EGFR to engage in autophosphorylation and thus enhance stimulatory ligand-binding events through oligomerization[32,33]. However, degradation of EGFR with **Ab-2** reduced phosphorylation, demonstrating the advantages of receptor removal. This effect was dependent on CI-M6PR (Extended Data Fig. 5h). Because downstream kinase phosphorylation is independent of EGFR phosphorylation in non-starved HeLa cells[34], we used Hep3B hepatocellular carcinoma cells. **Ab-2** facilitated robust EGFR degradation in Hep3B cells (Fig. 4h), and this degradation desensitized cells to EGF stimulation (Fig. 4i). Notably, although ctx treatment inhibited EGFR phosphorylation, levels of downstream phosphorylated Akt (pAkt) were similar between ctx and untreated cells. Only with **Ab-2** treatment was downstream pAkt reduced to the levels observed in unstimulated cells. Proliferation of HepG2 cells is known to be stimulated by EGF[35]. We showed that **Ab-2** inhibited the proliferative effects of EGF stimulation in HepG2 cells, relative to treatment with ctx alone (Extended Data Fig. 7a, b).

To demonstrate the scope of the LYTAC platform, we targeted several additional membrane-associated proteins for degradation. CD71 (transferrin receptor-1)–a therapeutic cancer target that is progressing towards clinical trials–is known to cycle between early endosomes and the cell surface, avoiding trafficking to the lysosome for degradation[36]. Upon incubation of Jurkat cells with a mouse anti-CD71 antibody and **Ab-1** (Fig. 4j), degradation of CD71 was observed (greater than 80%; Fig. 4k), which was dependent on M6Pn recognition (Extended Data Fig. 8g). Note that the anti-CD71 antibody alone is reported to induce partial CD71 downregulation[37]. After 24-h incubation, cells treated with anti-CD71 and **Ab-1** internalized less transferrin-647 than did untreated cells or cells treated with non-M6Pn-bearing antibodies (Fig. 4l), further highlighting the functional consequences of target degradation.

Additionally, we investigated whether LYTACs could degrade PD-L1, a driver of cancer cell immune evasion. For PD-L1 to undergo accelerated degradation, the LYTAC must overcome the PD-L1 recycling pathway[38]. MDA-MB-231 cells–which are PD-L1-positive–were treated with anti-PD-L1, anti-PD-L1 functionalized with GalNAc glycopolypeptides or anti-PD-L1-M6Pn LYTAC (**Ab-3**, Extended Data Fig. 8a). Treatment with **Ab-3** resulted in a significant decrease (average 33%) in cell-surface PD-L1 levels compared to treatment with unfunctionalized anti-PD-L1 or anti-PD-L1-poly(GalNAc) (Extended Data Fig. 8b, c). As MDA-MB-231 cells express low levels of CI-M6PR, we tested the degradation of PD-L1 in the Hodgkin's lymphoma cell line HDLM-2, which expresses higher levels of CI-M6PR. After 36 h of treatment with **Ab-3**, 50% downregulation of total PD-L1 was observed

(Extended Data Fig. 8d, e). When treated with a LYTAC derived from atezolizumab (the active ingredient in Tecentriq) (Extended Data Fig. 8f)–an FDA-approved PD-L1-blocking antibody–we observed a greater extent of PD-L1 degradation (average 70% degradation, Fig. 4m), which was dependent on M6Pn-recognition (Fig. 4n). Thus, LYTACs can override the endogenous recycling programs of cell-surface proteins and accelerate their lysosomal degradation.

Finally, we asked how M6Pn conjugation might affect antibody clearance in vivo. BALB/c mice were injected intraperitoneally with 5 mg kg^{-1} ctx or ctx-M6Pn, and serum antibody levels were assayed by western blotting. Six hours after injection, we observed a threefold reduction in serum ctx-M6Pn relative to ctx, suggesting a rapid clearance phase post-injection (Fig. 4o, p). However, between 6 h and 72 h we observed only a moderate decrease in serum ctx-M6Pn relative to ctx, and no substantial accumulation in either the liver or the spleen (Extended Data Fig. 9). These data suggest two regimes of clearance: a rapid initial phase and a slower, more sustained clearance. Modulating these two regimes will be important for tailoring the in vivo efficacy of any individual combination of LYTAC and target protein.

In summary, the LYTAC platform enables targeting of extracellular and membrane-associated proteins directly for lysosomal degradation. The success of a particular LYTAC is likely to result from a combination of factors–including the endogenous kinetics of protein trafficking and turnover, the amount of surface localization, the inherent susceptibility to lysosomal transportation through clathrin-mediated endocytosis and the stoichiometry relative to the lysosome-targeting receptor. Although the LYTACs described above take advantage of CI-M6PR, in principle other shuttling receptors could be co-opted, reducing the potential for resistance to develop when targeting oncoproteins. We have demonstrated that both small molecules and larger peptides can be used as protein target binders in LYTACs. Modulating the pharmacokinetic properties to control off-target clearance and stoichiometries of a given LYTAC necessary to effectively degrade a membrane protein will remain a key challenge for further translational applications. We anticipate that the chemical tunability and modularity of LYTACs will offer new opportunities to manipulate these parameters for targeted protein degradation of secreted and membrane proteins, both for research and for potential therapeutics.

Online content

Any methods, additional references, Nature Research reporting summaries, source data, extended data, supplementary Information, acknowledgements, peer review information; details of author contributions and competing interests; and statements of data and code availability are available at https://doi.org/10.1038/s41586-020-2545-9.

Methods

Data reporting

No statistical methods were used to predetermine sample size. The experiments were not randomized and the investigators were not blinded to allocation during experiments and outcome assessment.

General synthetic chemistry procedures

All reactions were performed in standard, dry glassware fitted with rubber septa under an inert atmosphere of nitrogen unless otherwise described. Reagents were purchased in reagent grade from commercial suppliers and used as received, unless otherwise described. Anhydrous solvents (acetonitrile, benzene, dichloromethane, diethyl ether, *N*,*N*-dimethylformamide, tetrahydrofuran and toluene) were prepared by passing the solvent through an activated alumina column. See the Supplementary Information for detailed synthetic procedures and characterization of all new compounds.

Cell lines

Cells were grown in T75 flasks (Thermo Fisher) and maintained at 37 °C and 5% CO_2. K562 and Jurkat cells were grown in RPMI supplemented with 10% fetal bovine serum (FBS) and 1% penicillin/streptomycin. THP-1 cells were grown in RPMI supplemented with 10% FBS, 1% penicillin/streptomycin, and 0.05 mM 2-mercaptoethanol. HeLa, MDA-MB-361, HEK-293, HEK-293T, Hep3B and MDA-MB-231 cells were grown in DMEM supplemented with 10% FBS and 1% penicillin/streptomycin. HepG2 cells were grown in low-glucose DMEM supplemented with 10% FBS and 1% penicillin/streptomycin. BT474 cells were grown in RPMI supplemented with 10% FBS and 1% penicillin/streptomycin with 0.023 U ml^{-1} insulin. HDLM-2 cells were grown in RPMI supplemented with 20% heat-inactivated FBS and 1% penicillin/streptomycin. HeLa and K562 cells stably expressing dCas9-KRAB were a gift from M. Bassik. Jurkat, HeLa, MDA-MB-361, MDA-MB-231, THP-1, K562, HEK-293, HEK-293T, Hep3B, HepG2 and BT474 cells were obtained from the American Type Culture Collection (ATCC), HDLM-2 cells were obtained from the laboratory of T. Waldmann. Cell lines were authenticated by the supplier. Cell lines were verified to be mycoplasma-negative using a Lonza MycoAlert Mycoplasma Detection Assay.

General procedure for NeutrAvidin-647 uptake experiments

Cells (70% confluent in 24-well plate for adherent cells, 1×10^6 cells per ml for suspension cells) were incubated in complete growth medium supplemented with 500 nM NA-647, or NA-647 and 2 μM glycopolypeptide. Addition was performed sequentially, with NA-647 added first followed by glycopolypeptide and immediate transfer to 37 °C.

General procedure for protein uptake and degradation experiments

Cells (70% confluent in 24-well plate for adherent cells, 2×10^6 cells per ml for suspension cells) were incubated in complete growth medium supplemented with 50 nM target protein, or 50 nM target protein and 25 nM of each antibody. Addition was performed sequentially,

with target protein added first followed by secondary antibodies, followed by primary antibodies, and subsequent immediate transfer to 37 °C. Recombinant proteins were expressed in-house (mCherry) or purchased from Abcam (human apolipoprotein E4, ab50243) and labelled with commercially available fluorescent dyes.

CRISPRi screen procedure

The hCRISPRi-v2 library was a gift from J. Weissman (Addgene ID 83969). K562 cells stably expressing dCas9-KRAB were infected with the 104,535 sgRNA library described previously[27], targeting the transcriptional start sites of 18,905 annotated genes at a redundancy of 5 sgRNA per start site. Infectivity was titrated such as to transduce the library at a multiplicity of infection of 0.3–0.4. Cells were selected with puromycin for 96 h and then allowed to expand in puromycin-free media for 48 h. Staining and FACS was performed within seven days of completion of puromycin selection. On the day of sorting, two replicates of 50×10^6 library-infected cells (4×10^6 cells per ml) were incubated with NA-647 (500 nM) and poly(M6Pn)$_{long}$ (2 μM) for 1 h at 37 °C. Cells were washed three times with PBS at 4 °C. Cells were then resuspended in PBS with SYTOX Green (according to the manufacturer's specifications) and sorted by FACS using a BD Aria II. Intact, viable cells were selected by gating on FSC/SSC and SYTOX Green channels. A population of cells representing the bottom 15% of the fluorescence distribution in the NA-647 channel was then selected for and sorted. Sorting was conducted until 25×10^6 events had been processed, corresponding to an approximately 250-fold library coverage. Sorted cells were then pelleted and frozen for subsequent downstream processing. Aliquots of 50×10^6 unsorted cells from each replicate were also pelleted and frozen down in parallel for normalization.

CRISPRi screen DNA extraction and data analysis

Frozen cell pellets were thawed and genomic DNA extraction was performed using either the QIAamp DNA Blood Maxi Kit (for unsorted samples) or the Sigma GeneElute Mammalian Genomic DNA Miniprep kit (for sorted samples) according to manufacturer's specifications. The sgRNA-encoding regions were amplified via nested PCR and sequenced on an Illumina NextSeq500. Alignment of sequencing reads to the sgRNA library and statistical comparison of positively selected genes in sorted versus unsorted samples was performed using MaGeCK[39]. MaGeCK returned a statistical score for gene enrichment in the sorted population and genes were ranked by a positive selection score corresponding to the −log(PosScore). GO enrichment analysis was performed using GOrilla[40].

Generation of CRISPRi-knockdown cell lines

K562 or HeLa cells stably expressing dCas9-KRAB were infected with lentivirus-encoding sgRNAs identified from the CRISPRi screen. Lentivirus was produced by co-transfection of HEK-293T cells with a lentiviral transfer vector and packaging plasmids (pGag/pol, pREV, pTAT, pVSVG). Transfection was performed using Lipofectamine 2000 reagent as recommended by the manufacturer. Viral supernatants were collected 48 h after transfection, filtered through a 0.45-μm filter, and added to target cells (400 μl viral supernatant per well in a 6-well plate) along with polybrene (8 μg per ml). Then, 48 h post infection, cell media was replaced and cells were placed under puromycin selection (2 μg ml^{-1}).

sgRNA guides: *IGF2R* 5′-GAGGTGAGCGCGGCTCGACT-3′; *EXOC1* 5′-GGGCGGACAGACGAGCTGAC-3′; *EXOC2* 5′-GGGCGGAAGTGA GGTGCCGG-3′; non-targeting (*GAL4*) 5′-GTTGGAGCACTGTC CTCCGAACGT-3′.

Flow cytometry for surface staining and uptake measurements

For protein uptake experiments in suspension cell lines, cells were incubated for the indicated time with proteins and conjugates, then washed 3 times with PBS at 4 °C. Cells were then incubated with either SYTOX Green or SYTOX Red according to the manufacturer's specifications for 15 min on ice. For protein uptake experiments in adherent cell lines, cells were incubated for the indicated time with proteins and conjugates, then washed two times quickly with PBS and lifted with trypsin. Cells were transferred to a 96-well V-bottom plate and washed 3 times with PBS, then incubated with either SYTOX Green or SYTOX Red according to the manufacturer's specifications for 15 min on ice. For surface-staining experiments, adherent cells were lifted with non-enzymatic cell dissociation buffer (Gibco) and transferred to a 96-well V-bottom plate, and suspension cells were transferred to a 96-well V-bottom plate. After washing 3 times with 0.5% BSA in PBS, cells were incubated with primary antibody for 30 min on ice. Cells were subsequently washed 3 times with 0.5% BSA in PBS, then incubated with secondary antibodies for 30 min on ice. After incubation, cells were washed 3 times with 0.5% BSA in PBS and incubated with either SYTOX Green or SYTOX Red according to the manufacturer's specifications for 15 min on ice. Flow cytometry was performed on either a BD-Accuri C6 Plus or DxP FACScan flow cytometer, and analysis was performed using the FlowJo software package. Gating was performed on single cells and live cells.

Cell surface degradation experiment

Adherent cells (70% confluency for 24-h experiments, 50% confluency for 48-h experiments) were treated with antibodies or conjugates in complete growth medium. At the indicated time, cells were washed three times with Dulbecco's phosphate-buffered saline (DPBS), then lysed as detailed below. Suspension cells were suspended in complete growth media in a flat bottom plate, and at the indicated time transferred to a 96-well V-bottom plate and washed three times with PBS, then lysed as detailed in 'Western blotting'.

Competitive EGF stimulation experiment

Adherent cells (70% confluency for 24-h experiments, 50% confluency for 48-h experiments) were treated with antibodies or conjugates in complete growth medium. At the indicated time, cells were washed three times with DPBS, then incubated with EGF in fresh complete growth medium. After incubation, cells were washed three times with DPBS, then lysed as detailed in 'Western blotting'.

Western blotting

Cell culture experiments with adherent cells conducted in 24-well plates were washed 3 times with DPBS, then lysed with RIPA buffer supplemented with protease inhibitor cocktail (Roche), phosphatase inhibitor cocktail (Cell Signaling Technologies) and 0.1% benzonase (Millipore-Sigma) on ice for 30 min. The lysates were spun at 21,000g for 15 min at 4 °C

and protein concentration was determined using BCA assay (Pierce). Suspension cell lines were transferred to a 96-well V-bottom plate, washed 3 times with PBS, then lysed with RIPA buffer supplemented as above. Adherent cells in 6-well plates were washed three times with DPBS then lysed with 1X Laemmli buffer containing protease inhibitor cocktail (Roche) and phosphatase inhibitor cocktail (Cell Signaling Technologies). Lysates were then sonicated on ice using a microtip sonicator for 30 s, with 10 s sonication intervals and rest intervals, and protein concentration was determined using BCA assay (Pierce). Equal amounts of lysates were separated by SDS–PAGE (4–12% Bis-Tris gel or 10% Bis-Tris gel), then transferred to a nitrocellulose membrane. After transfer, the membrane was stained for total protein using REVERT Total Protein Stain (LI-COR), then blocked in TBS-T with 5% non-fat dried milk or Odyssey Blocking Buffer (TBS) (LI-COR) for 1 h at room temperature with gentle shaking. Membranes were incubated overnight with primary antibodies at 4 °C with gentle shaking, then washed three times with TBS-T for five minutes each. The membrane was then incubated with 800CW goat anti-mouse IgG, 800CW goat anti-rabbit IgG, 800CW donkey anti-goat IgG, 680LT goat anti-rabbit IgG or 680LT goat anti-mouse IgG secondary antibodies (1:10,000) in Odyssey Blocking Buffer (TBS) for 1 h at room temperature with gentle shaking. Membranes were washed three times with TBS-T, then imaged using an OdysseyCLxImager (LI-COR). Quantification of band intensities was performed using Image Studio Software (LI-COR).

Confocal microscopy

A Nikon A1R confocal microscope equipped with a Plan Fluor 60× oil immersion 1.30– numerical aperture objective was used. This instrument is equipped with a 405-nm violet laser, a 488-nm blue laser, a 561-nm green laser and a 639-nm red laser.

Mass spectrometry

Sample preparation.—Samples were prepared for proteomic analysis using a previously described method with methanol precipitation to extract proteins, followed by tryptic digestion[41]. In brief, HeLa cells from each treatment condition were lysed by suspension in 6 M guanidine, total protein concentration was measured using BCA (Thermo Fisher Scientific), and 100 μg of protein was extracted via precipitation in 90% methanol for each sample. Supernatants were decanted and protein pellets were suspended in a buffer comprising 8 M urea, 100 mM Tris pH 8, 10 mM tris(2-carboxyethyl)phosphine and 40 mM chloroacetamide. After incubation at room temperature for 30 min, samples were diluted to 1.5 M urea with 100 mM Tris pH 8 and digested with trypsin (50:1 protein to enzyme, Promega) overnight. Sample cleanup was performed by first quenching with formic acid to a final pH of around 2, followed by desalting over a polystyrene–divinylbenzene solid phase extraction (PS–DVB SPE) cartridge (Phenomenex). Samples were dried with vacuum centrifugation after desalting, and peptide mass was assayed using a peptide colorimetric assay (Fisher).

LC–MS/MS.—All samples were resuspended in 0.2% formic acid in water at around 500 ng μl^{-1}, and 500 ng of total peptide mass was injected on column for each sample. Peptides were separated over a 25-cm EasySpray reversed phase LC column (75 μm inner diameter packed with 2 μm, 100 Å, PepMap C18 particles, Thermo Fisher Scientific). The mobile

phases (A: water with 0.2% formic acid and B: acetonitrile with 0.2% formic acid) were driven and controlled by a Dionex Ultimate 3000 RPLC nano system (Thermo Fisher Scientific). Gradient elution was performed at 300 nl min^{-1}. Mobile phase B was increased to 5% over 6 min, followed by an increase to 40% at 76 min, a ramp to 90% B at 77 min, and a wash at 90% B for 10 min. Flow was then ramped back to 0% B over the course of 1 min, and the column was re-equilibrated at 0% B for 12 min, for a total analysis of 100 min. Eluted peptides were analysed on an Orbitrap Fusion Tribrid MS system (Thermo Fisher Scientific). Precursors were ionized using an EASY-Spray ionization source (Thermo Fisher Scientific) source held at +2.2 kV compared to ground, and the column was held at 40 °C. The inlet capillary temperature was held at 275 °C. Survey scans of peptide precursors were collected in the Orbitrap from 350-1500 Th with an automatic gain control target of 1,000,000, a maximum injection time of 50 ms and a resolution of 120,000 at 200 *m/z*. Monoisotopic precursor selection was enabled for peptide isotopic distributions, precursors of $z = 2–5$ were selected for data-dependent MS/MS scans for 2 s of cycle time, and dynamic exclusion was set to 45 s with a ±10 ppm window set around the precursor monoisotope. An isolation window of 0.7 *m/z* was used to select precursor ions with the quadrupole. MS/MS scans were collected using high-energy collisional dissociation at 30 normalized collision energy (nce) with an automatic gain control target of 30,000 and a maximum injection time of 25 ms. Mass analysis was performed in the linear ion trap using the ‘Rapid’ scan speed while scanning from 200–1,500 *m/z*.

Data analysis.—Raw data were processed using MaxQuant version 1.6.3.4[42], and tandem mass spectra were searched with the Andromeda search algorithm[43]. Oxidation of methionine and protein N-terminal acetylation were specified as variable modifications, while carbamidomethylation of cysteine was set as a fixed modification. A precursor ion search tolerance of 20 ppm and a product ion mass tolerance of 0.3 Da were used for searches, and two missed cleavages were allowed for full trypsin specificity. Peptide spectral matches were made against a target-decoy human reference proteome database downloaded from Uniprot. Peptides were filtered to a 1% FDR and a 1% protein FDR was applied according to the target-decoy method[44]. Proteins were identified and quantified using at least one peptide (razor + unique), where razor peptide is defined as a non-unique peptide assigned to the protein group with the most other peptides (Occam’s razor principle). Proteins were quantified and normalized using MaxLFQ[45] with a label-free quantification (LFQ) minimum ratio count of 1. LFQ intensities were calculated using the match between runs feature, and MS/MS spectra were required for LFQ comparisons. For quantitative comparisons, protein intensity values were log_2-transformed before further analysis, and missing values were imputed from a normal distribution with width 0.3 and downshift value of 1.8 (that is, default values) using the Perseus software suite[46]. Significance calculations were performed using a two-tailed *t*-test with heteroscedastic variance (performed in Microsoft Excel).

Antibody in vivo clearance study

Mouse experiments were performed in compliance with ethical regulations approved by the Administrative Panel on Laboratory Animal Care (APLAC) at Stanford University under protocol 31511. Female BALB/c mice (6–8 weeks old, from the Jackson Laboratory) were

treated with 5 mg kg^{-1} of either antibody or conjugate via intraperitoneal injection (3 mice per group). The initial grouping of mice was random, after which no additional randomization or blinding was used. At the indicated time, blood was sampled from the tail using anti-coagulant capillary tubes, and serum was separated after centrifugation at 700*g* at 4 °C for 15 min. To analyse the presence of human antibody in serum, 2 μl serum was diluted into 30 μl LDS loading buffer and separated by SDS–PAGE (4–12% or 10% Bis-Tris gel), then transferred to a nitrocellulose membrane. Liver and spleen were collected after 72 h, homogenized and lysed with RIPA buffer supplemented with protease inhibitor cocktail and 0.1% benzonase, and 50 ug of organ lysate were separated by SDS–PAGE (4–12% Bis-Tris gel). The presence of cetuximab was detected using 800CW goat anti-human IgG secondary antibody (1:1,000).

Reporting summary

Further information on research design is available in the Nature Research Reporting Summary linked to this paper.

Extended Data

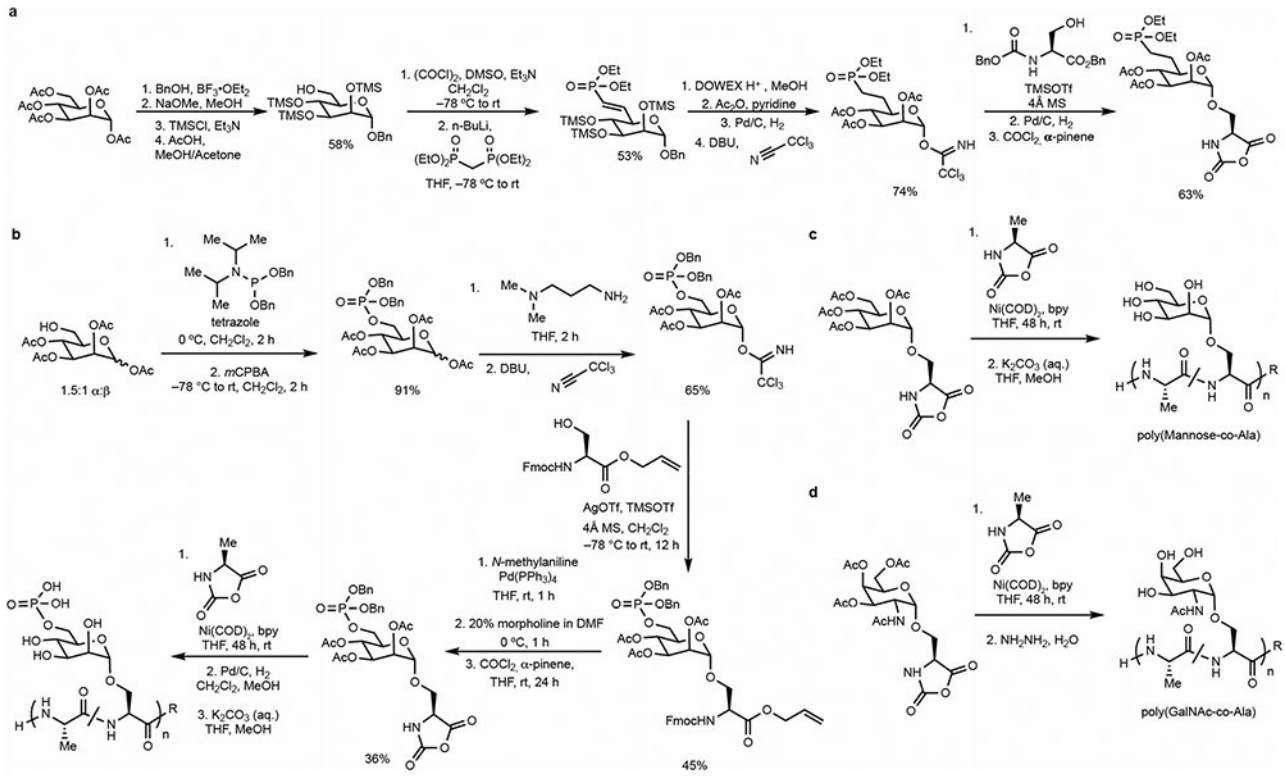

Extended Data Fig. 1 |. Synthesis of M6Pn-NCA, poly(mannose-6-phosphate-co-Ala), poly(mannose-co-Ala) and poly(GalNAc-co-Ala).

a, Synthetic route to mannose-6-phosphonate-serine *N*-carboxyanhydride (NCA). **b**, Synthetic route to M6P-NCA, followed by Ni-catalysed polymerization. Polymerization reactions were carried out in a N_2 glovebox for 48 h in tetrahydrofuran. **c**, **d**, General synthetic schemes for the polymerization of mannose-NCA (**c**) and GalNAc-NCA (**d**). DBU,

1,8-diazabicyclo[5.4.0]undec-7-ene; Fmoc, fluorenylmethyloxycarbonyl; mCPBA, *meta*-chloroperoxybenzoic acid; OTf, triflate.

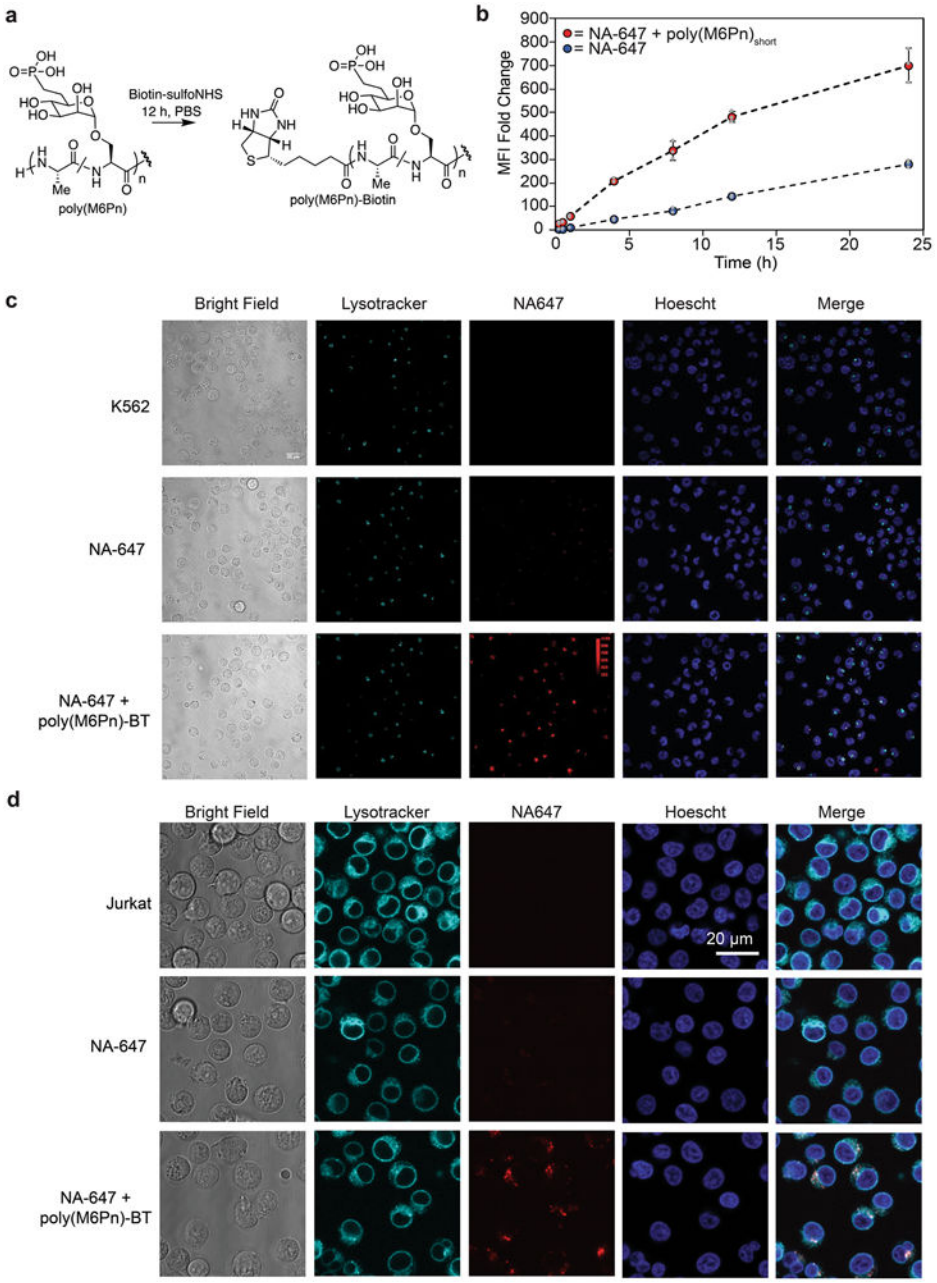

Extended Data Fig. 2 |. Biotin-poly(M6Pn) LYTACs direct NA-647 to lysosomes.
a, General scheme for biotinylation of glycopolypeptides with sulfo-NHS biotin. Biotinylation reactions were performed in 1× PBS at room temperature overnight. **b**, Biotin–LYTAC-mediated NA-647 uptake is continuous over time in K562 cells. K562 cells were incubated at 37 °C in complete growth medium with 500 nM NA-647 or 500 nM NA-647 and 2 μM poly(M6Pn)$_{short}$ for the indicated time, then washed and analysed by live-cell flow cytometry. The MFI (mean fluorescence intensity) was measured relative to background

fluorescence from untreated K562 cells. **c**, **d**, Biotinylated poly(M6Pn) LYTACs direct NA-647 to lysosomes in K562 cells (**c**) and Jurkat cells (**d**). Cells were incubated with PBS, 500 nM NA-647, or 500 nM NA-647 and 2 μM biotinylated poly(M6Pn)$_{short}$ for 0.5–1 h in complete growth medium. NA-647 (red) colocalized with acidic endosomes and lysosomes as labelled with LysoTracker Green (turquoise). Scale bar, 20 μm. Fluorescence intensity is normalized in the NA-647 channel for all images. For **c**, **d**, data are representative of two independent experiments. For **b**, data are mean ± s.d. of three independent experiments.

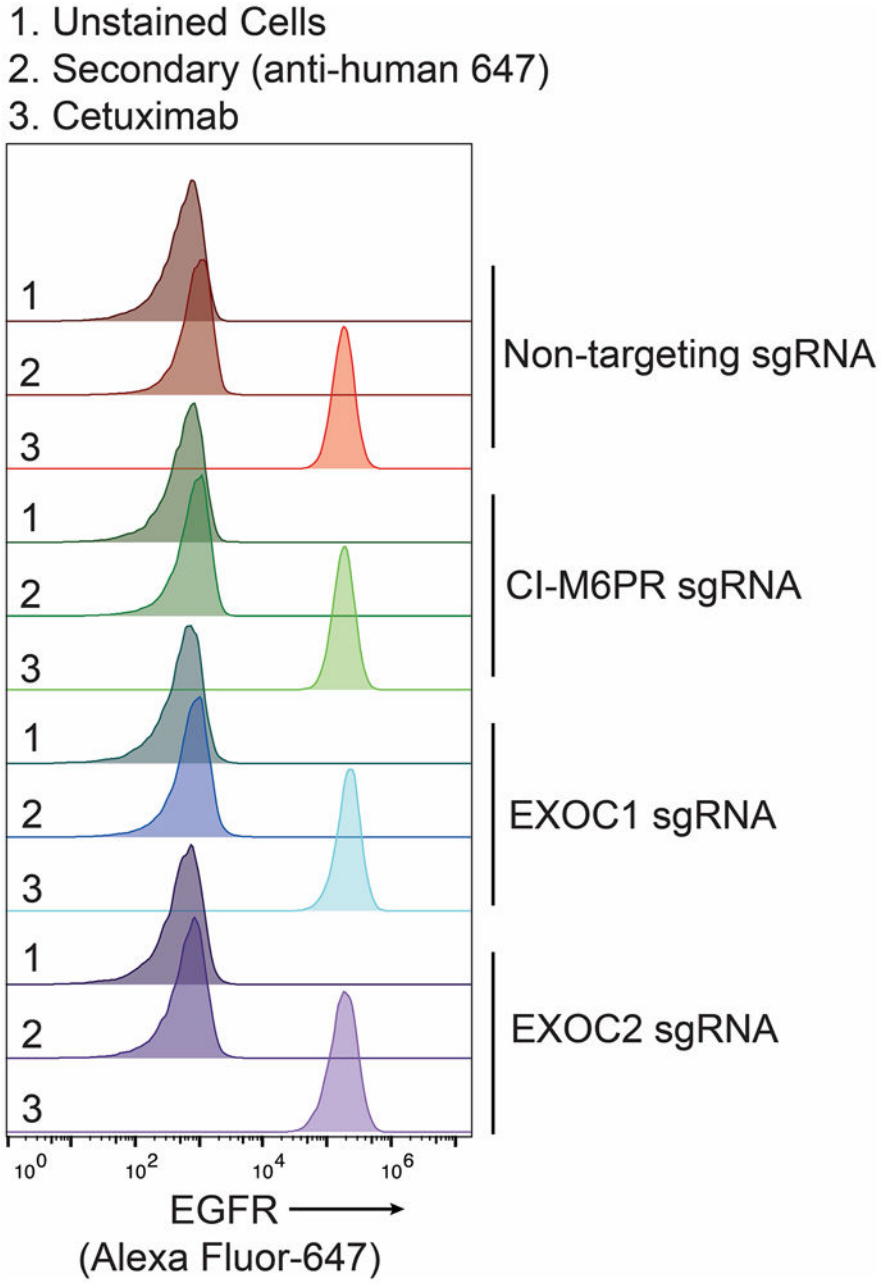

Extended Data Fig. 3 |. EGFR surface levels are unchanged upon *EXOC1* and *EXOC2* knockdown in HeLa cells.

Cetuximab binds equally to dCas9-KRAB HeLa cells transfected with non-targeting sgRNA and cells transfected with sgRNA targeting *IGF2R*, *EXOC1* or *EXOC2*, indicating no change in EGFR surface levels. Cells were subjected to live-cell flow cytometry using cetuximab followed by an anti-human Alexa Fluor-647-conjugated anti-human (anti-human 647) secondary antibody. Data are representative of two independent experiments.

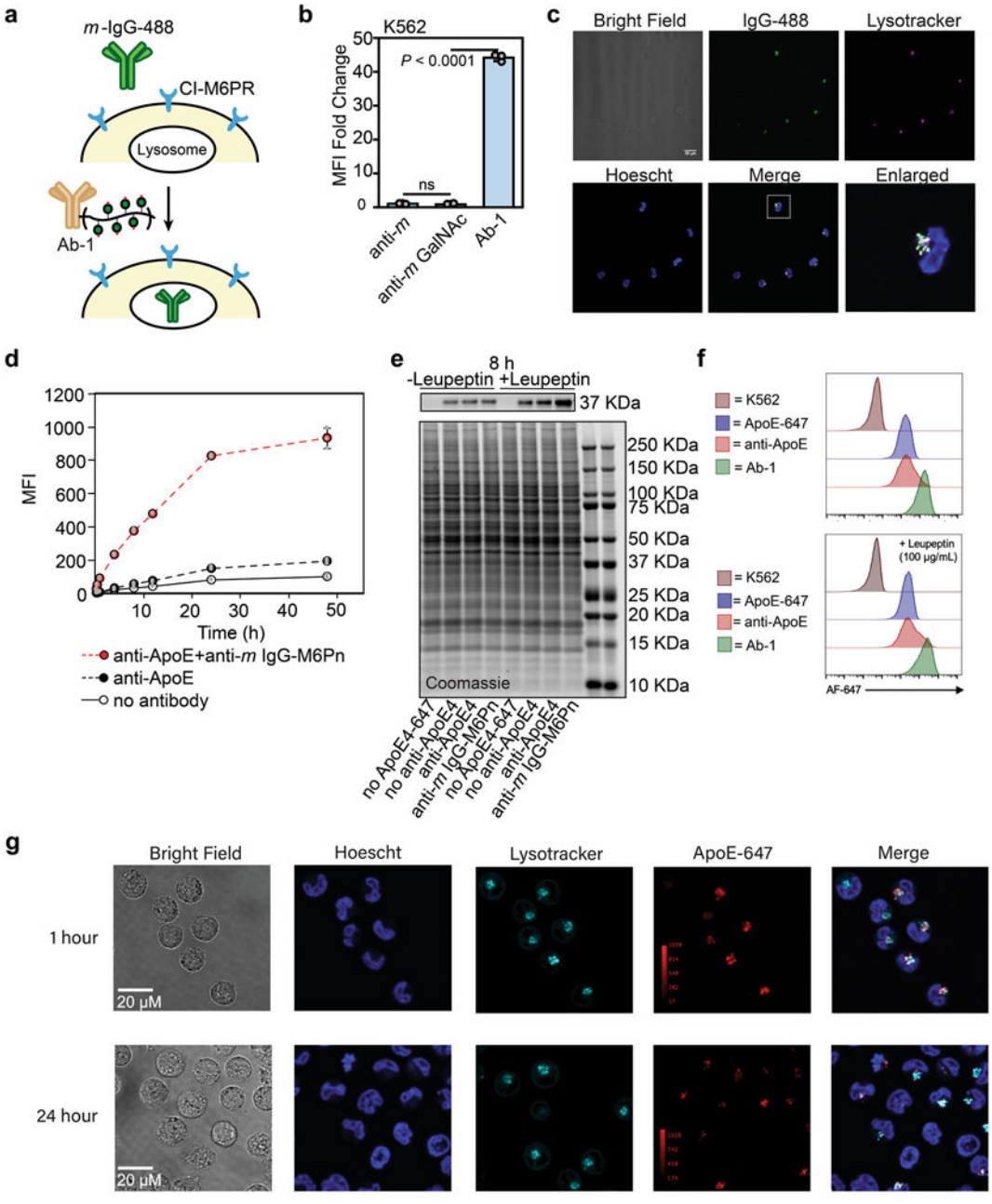

Extended Data Fig. 4 |. Ab-1 mediates uptake of soluble proteins to lysosomes.

a, Uptake of an Alexa Fluor-488 (AF488)-labelled mouse IgG (*m*-IgG-488) into cells using antibody LYTACs. **b**, Uptake of *m*-IgG-488 using **Ab-1**. Mean fluorescence intensity (MFI) fold change over background uptake measured by live-cell flow cytometry. K562 cells were

incubated at 37 °C for 1 h with 50 nM IgG-488 or 50 nM IgG and 25 nM of anti-mouse or **Ab-1**. **c**, AF488 signal (green) colocalized with acidic endosomes and lysosomes as labelled with LysoTracker Red (magenta). Expanded view shows a cell containing IgG-488 and LysoTracker Red. Scale bar, 20 μm. **d**, ApoE4-647 uptake over time. K562 cells were incubated with 50 nM ApoE4-647 in the presence or absence of 25 nM anti-ApoE4 and **Ab-1**. At the indicated time point, cells were aliquoted and median fold intensity (MFI) measurements were measured by live-cell flow cytometry. **e**, Total protein levels for leupeptin inhibition of apoE4 degradation in K562 cells, corresponding to lanes shown in Fig. 3h. Total protein was visualized by Coomassie stain. **f**, Flow cytometry plots of ApoE4-647 uptake over time, with or without leupeptin inhibition. **g**, Uptake of ApoE4-647 to lysosomes. K562 cells were incubated with PBS, 50 nM ApoE4-647, 25 nM anti-ApoE4 and 25 nM Ab-1 for 1 h or 24 h in complete growth media at 37 °C. Alexa Fluor-647 signal (red) colocalizes with acidic endosomes and lysosomes as labelled with LysoTracker Green (turquoise). Data are representative of two (**c**, **e**–**g**) independent experiments. Data are mean ± s.d. of three independent experiments (**b**, **d**). *P* values were determined by unpaired two-tailed *t*-tests; fold changes are reported relative to incubation with protein targets alone (**b**) or background fluorescence (**d**).

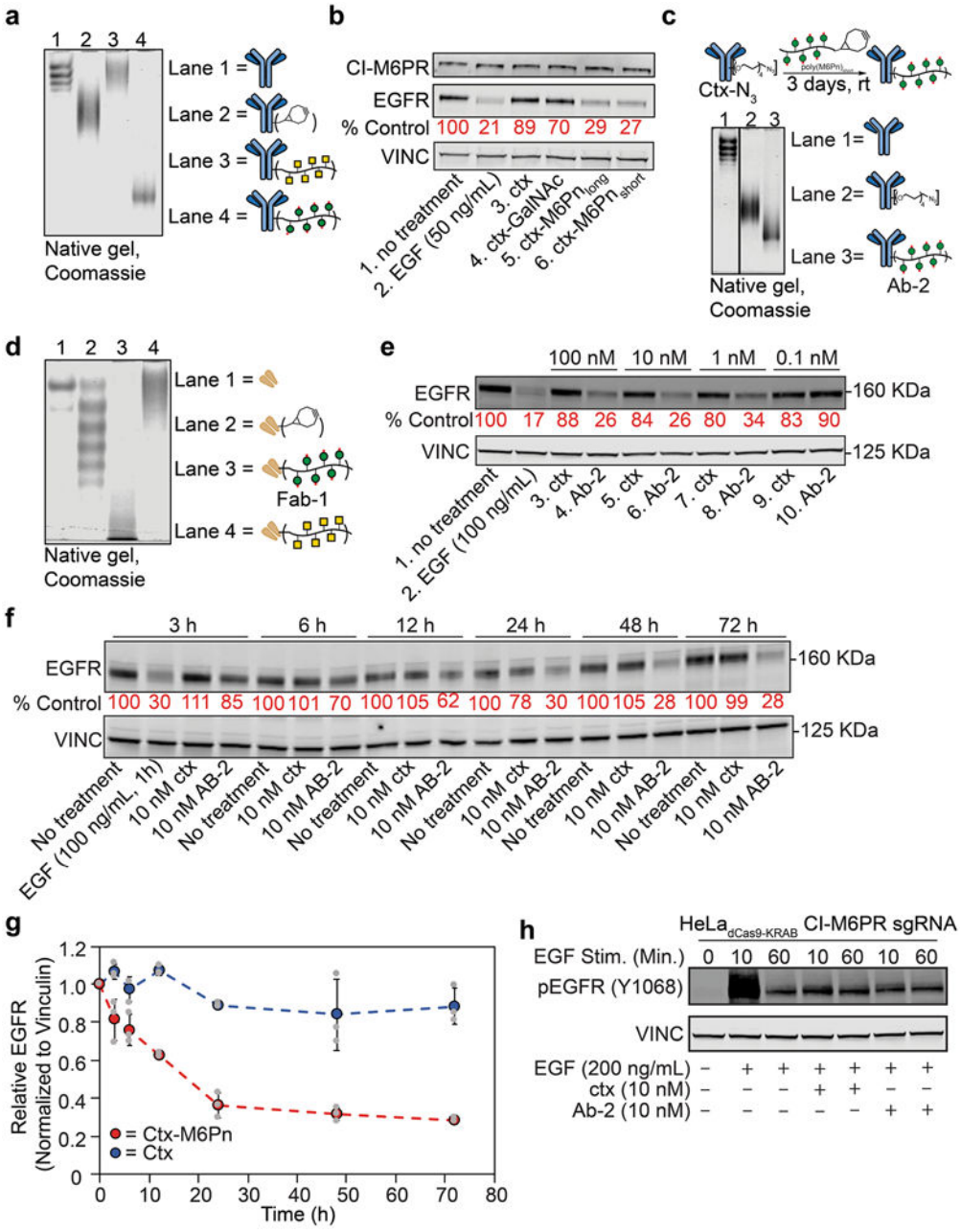

Extended Data Fig. 5 | Optimization of LYTAC-mediated EGFR degradation.

a, Native gel of cetuximab (ctx)-based LYTACs. **b**, Levels of EGFR in HeLa cells treated with 100 nM ctx (lane 3), ctx-GalNAc (lane 4), ctx-M6Pn$_{long}$ (lane 5) or ctx-M6Pn$_{short}$ (lane 6) for 24 h in complete growth medium. EGF stimulation is a positive control for EGFR downregulation. **c**, Synthesis of linker-swapped **Ab-2**. Ctx was labelled with NHS-PEG$_4$-N$_3$, then incubated with BCN-functionalized poly(M6Pn)$_{short}$ for 3 days at room temperature. Reaction progress was monitored by native gel electrophoresis and visualized with Coomassie stain. **d**, Native gel of ctx-Fab-based LYTACs. **e**, EGFR levels in dCas9-KRAB HeLa cells transfected with non-targeting sgRNA against *GAL4* after incubation with 100 nM, 10 nM,1 nM, or 0.1 nM conjugates for 36 h in complete growth medium. **f**, EGFR

levels in dCas9-KRAB HeLa cells transfected with non-targeting *GAL4* sgRNA incubated with **Ab-2** or ctx for the indicated time. **g**, Quantification of LYTAC or ctx-mediated EGFR degradation in dCas9-KRAB HeLa expressing *GAL4* sgRNA over time as read out by western blot relative to untreated cells. **h**, Levels of pEGFR in dCas9-KRAB HeLa cells expressing an sgRNA targeting *IGF2R* after 24 h incubation with 10 nM ctx or **Ab-2**, then incubation with EGF for 10 or 60 min. Data are representative of two (**a**–**e**, **h**) or three (**f**) independent experiments. For **g**, data are mean ± s.d. of three independent experiments, one of which is shown in **f**. Per cent control was calculated by densitometry and normalized to loading control (**b**, **e**, **f**).

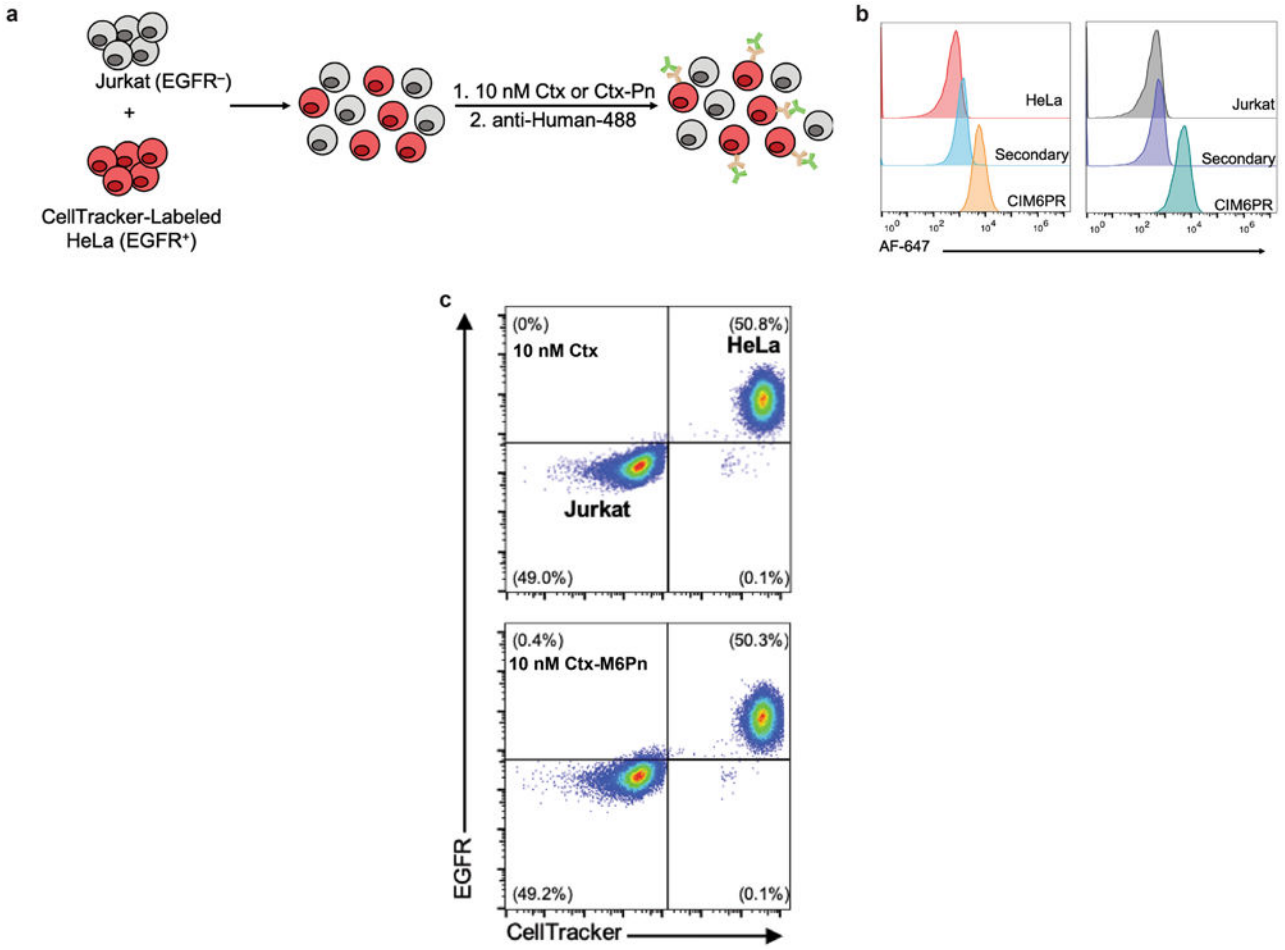

Extended Data Fig. 6 |. Mixed-cell assay demonstrates that binding specificity is comparable between ctx-M6Pn and ctx.

a, Scheme for mixed cell assay. HeLa cells were lifted and labelled with CellTracker Deep Red, then mixed in a 1:1 ratio with Jurkat cells. The mixed cell sample was stained with either 10 nM ctx or ctx-M6Pn conjugate, followed by anti-human 488, then subjected to live-cell flow cytometry. **b**, Cell surface CI-M6PR levels on HeLa cells ($CIM6PR^+EGFR^+$) and Jurkat cells ($CIM6PR^+EGFR^-$) were measured by live-cell flow cytometry. HeLa and Jurkat cells exhibited similar levels of cell-surface CI-M6PR. **c**, Ctx and ctx-M6Pn exhibit equivalent binding to HeLa cells, and ctx-M6Pn exhibits minimal increased binding to

Jurkat cells relative to ctx. Data are representative of two independent experiments (**b**) or two experimental replicates (**c**).

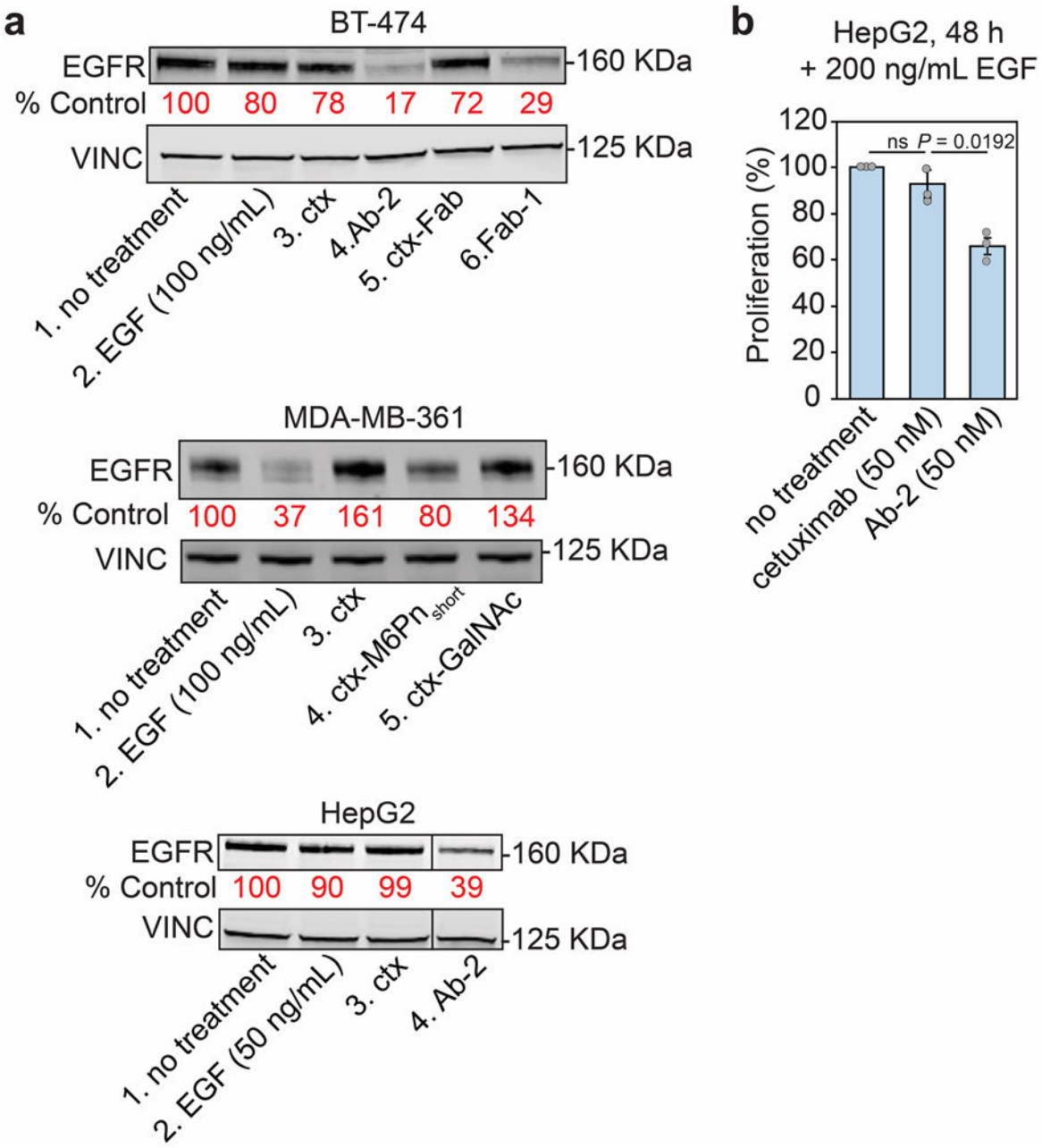

Extended Data Fig. 7 | LYTACs mediate EGFR degradation in multiple cell lines.
a, EGFR levels in BT-474, MDA-MB-361, or HepG2 cells after incubation with 10–20 nM conjugates. **b**, Proliferation of HepG2 cells in the presence of EGF (200 ng ml^{-1}) and 50 nM cetuximab or **Ab-2**. Cells were incubated with EGF and antibodies for 48 h, and proliferation measured using an MTS assay. Data are representative of three independent experiments (**a**). For **b**, data are mean ± s.e.m. of three independent experiments. *P* values

were determined by unpaired two-tailed *t*-tests. Per cent control was calculated by densitometry and normalized to loading control.

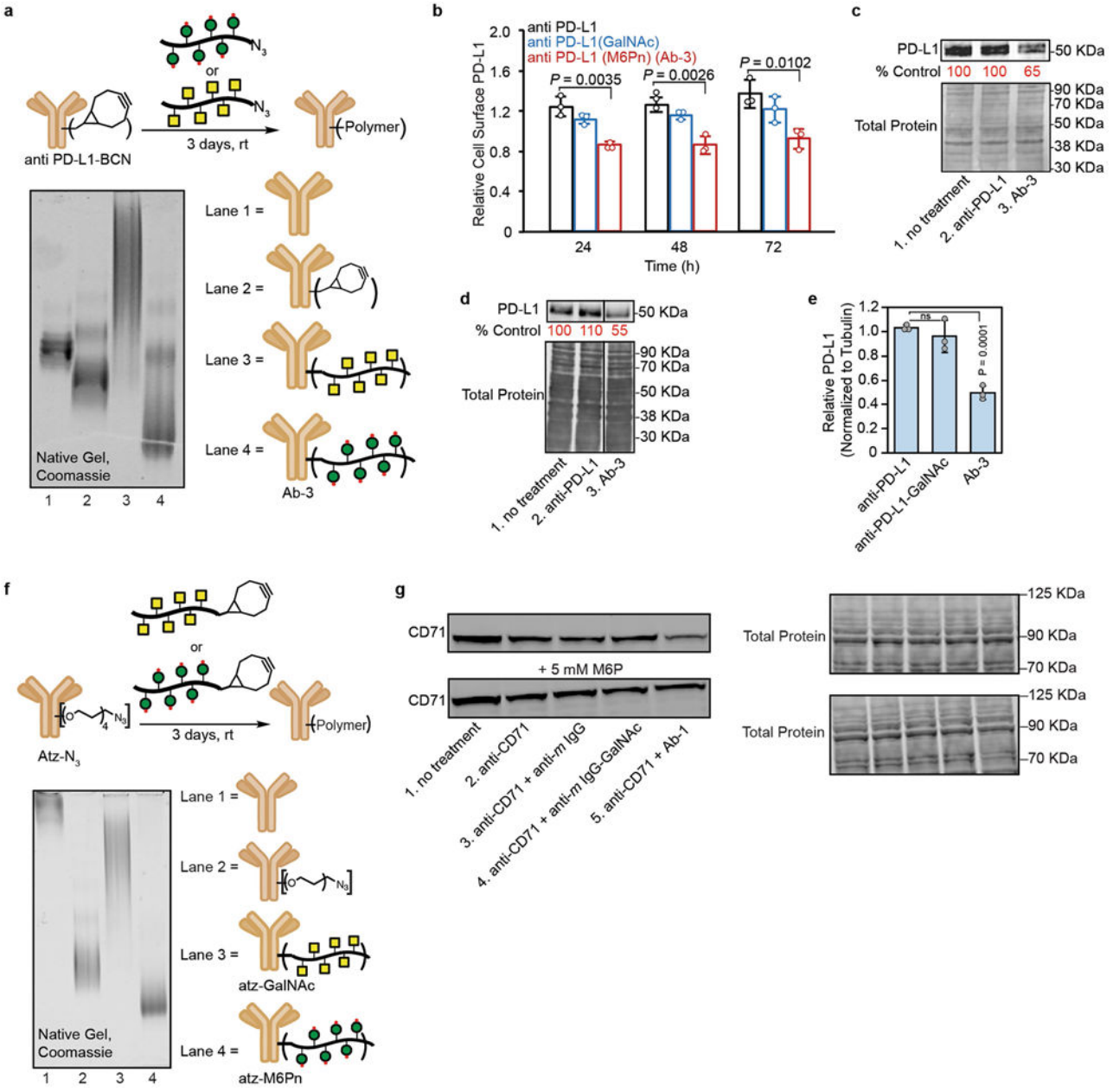

Extended Data Fig. 8 |. Synthesis of anti PD-L1 glycopolypeptide conjugates, PD-L1 degradation, and CD71 degradation depends on M6P binding.

a, Anti-PD-L1 was non-specifically labelled with BCN, then incubated with poly(M6Pn)$_{short}$ for 3 days at room temperature. Reaction progress was monitored by native gel electrophoresis and visualized by Coomassie stain. **b**, Cell-surface PD-L1 determined by live-cell flow cytometry after incubation with anti-PD-L1 or conjugates (50 nM). At each time point, cells were washed, lifted, brought to 4 °C, then stained for PD-L1 using excess unconjugated anti-PD-L1 (1 μM). **c**, PD-L1 levels in MDA-MB-231 cells after 48-h

incubation with anti-PD-L1 or **Ab-3. d**, PD-L1 levels in HDLM-2 cells after 36 h incubation with anti-PD-L1 or **Ab-3. e**, Quantification of PD-L1 degradation in HDLM-2 cells with **Ab-3**. **f**, Atezolizumab was non-specifically labelled with NHS-$(PEG)_4$-N_3, then incubated with poly$(M6Pn)_{short}$-BCN for 3 days at room temperature. Reaction progress was monitored by native gel electrophoresis and visualized by Coomassie stain. **g**, Levels of CD71 in Jurkat cells after 24 h in the presence of 5 mM M6P. Data are representative of two (**a**, **c**, **f**, **g**) independent experiments. For **b**, data are mean ± s.d. of three independent experiments, and cell surface levels are relative to untreated cells. For **e**, data are mean ± s.d. of three independent experiments, one of which is shown in **d**. Per cent control was calculated by densitometry and normalized to loading control.

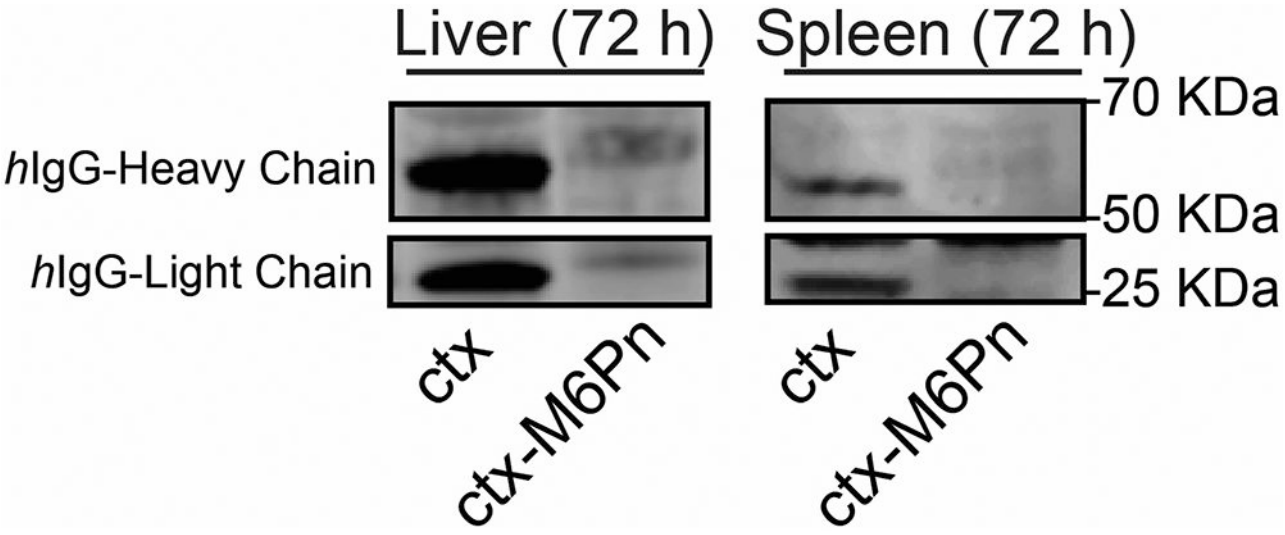

Extended Data Fig. 9 |. Human IgG in select mouse tissues.
Livers and spleens were collected from mice 72 h after intraperitoneal injection of ctx or ctx-M6Pn. Data are representative of three independent groups, one mouse per treatment per group.

Extended Data Table 1 |

Selected examples of proteins with differential abundance after treatment of HeLa cells with ctx or Ab-2

	Ab-2 (ctx-M6Pn)	
	Downregulated	
	Fold Change	p value
DHPR	−3.08	0.023
TFDP1	−2.98	0.039
8ODP	−1.82	0.019
CD99	−1.8	0.051
UBXN6	−1.55	0.043
WDR11	−1.38	0.049

Ab-2 (ctx-M6Pn)		
Downregulated		
	Fold Change	**p value**
BAG5	−1.35	0.015
AGAP3	−1.31	0.036
SCO2	−1.21	0.017
ORC2	−1.08	0.015
Upregulated		
	Fold Change	**p value**
CCD57	3.82	0.046
PGM2L	2.72	0.012
NFIB	2.48	0.003
ALKB5	2.21	0.029
COPRS	2.13	5.4E-05
IGKC	1.99	0.009
FRYL	1.99	0.024
DESP	1.12	0.0006
Cetuximab		
Downregulated		
	Fold Change	**p value**
TF2B	−2.37	0.008
HIF1N	−1.54	0.042
Upregulated		
	Fold Change	**p value**
CCD57	3.82	0.036
IGKC	3.15	0.032
NFIB	2.43	0.006
PO2F1	2.06	0.03
NRBP	2.01	0.011

Untreated, ctx-treated, or **Ab-2**-treated HeLa cells were lysed, digested, and analysed by quantitative proteomics. Depicted are exemplary hits with fold change values reported relative to untreated samples. Proteins highlighted in grey were found in both ctx and **Ab-2** treated cells. For a full list, see Supplementary Information. Data are mean of three biological replicates. *P* values were determined by unpaired two-tailed *t*-tests with untreated cells.

Supplementary Material

Refer to Web version on PubMed Central for supplementary material.

Acknowledgements

We thank M. Bassik for the CRISPRi library and dCas9-KRAB-expressing cell lines; T. Waldmann for a gift of the HDLM-2 cell line and E. Appel for use of aqueous gel permeation chromatography equipment. This work was supported in part by National Institutes of Health (NIH) grant P30CA124435 using the Stanford Cancer Institute Proteomics/Mass Spectrometry Shared Resource and by NIH grant R01CA227942 to C.R.B. S.M.B was supported by a National Institute of General Medical Sciences F32 Postdoctoral Fellowship. K.P. was supported by a National Science Foundation Graduate Research Fellowship, a Stanford Graduate Fellowship, and the Stanford ChEM-H Chemistry/Biology Interface Predoctoral Training Program. S.W. was supported by a Banting Postdoctoral

Fellowship from the Canadian Institutes of Health. G.A. was supported by a National Science Foundation Graduate Research Fellowship. N.M.R. was supported by NIH grant K00CA21245403.

Data availability

CRISPRi screen results are provided in Supplementary Table 1, quantitative proteomics results are provided in Supplementary Table 2. The flow cytometry gating strategy is provided in the Supplementary Information. All data that supported the findings of this study are included and are also available from the corresponding author upon request. Source data are provided with this paper.

References

1. Sakamoto KM et al. Protacs: chimeric molecules that target proteins to the Skp1-Cullin-F box complex for ubiquitination and degradation. Proc. Natl Acad. Sci. USA 98, 8554–8559 (2001). [PubMed: 11438690]
2. Winter GE et al. Phthalimide conjugation as a strategy for in vivo target protein degradation. Science 348, 1376–1381 (2015). [PubMed: 25999370]
3. Nabet B et al. The dTAG system for immediate and target-specific protein degradation. Nat. Chem. Biol 14, 431–441 (2018). [PubMed: 29581585]
4. Clift D et al. A method for the acute and rapid degradation of endogenous proteins. Cell 171, 1692–1706.e18 (2017). [PubMed: 29153837]
5. Fan X, Jin WY, Lu J, Wang J & Wang YT Rapid and reversible knockdown of endogenous proteins by peptide-directed lysosomal degradation. Nat. Neurosci 17, 471–480 (2014). [PubMed: 24464042]
6. Naito M, Ohoka N & Shibata N SNIPERs—hijacking IAP activity to induce protein degradation. Drug Discov. Today Technol 31, 35–42 (2019). [PubMed: 31200857]
7. Uhlén M et al. Tissue-based map of the human proteome. Science 347, 1260419 (2015). [PubMed: 25613900]
8. Brown KJ et al. The human secretome atlas initiative: implications in health and disease conditions. Biochim. Biophys. Acta 1834, 2454–2461 (2013). [PubMed: 23603790]
9. Coutinho MF, Prata MJ & Alves S A shortcut to the lysosome: the mannose-6-phosphate-independent pathway. Mol. Genet. Metab 107, 257–266 (2012). [PubMed: 22884962]
10. Ghosh P, Dahms NM & Kornfeld S Mannose 6-phosphate receptors: new twists in the tale. Nat. Rev. Mol. Cell Biol 4, 202–213 (2003). [PubMed: 12612639]
11. Gary-Bobo M, Nirde P, Jeanjean A, Morère A & Garcia M Mannose 6-phosphate receptor targeting and its applications in human diseases. Curr. Med. Chem 14, 2945–2953 (2007). [PubMed: 18220730]
12. Igawa T, Haraya K & Hattori K Sweeping antibody as a novel therapeutic antibody modality capable of eliminating soluble antigens from circulation. Immunol. Rev 270, 132–151 (2016). [PubMed: 26864109]
13. Alon R, Bayer EA & Wilchek M Affinity cleavage of cell surface antibodies using the avidin-biotin system. J. Immunol. Methods 165, 127–134 (1993). [PubMed: 8409464]
14. Liu L, Lee W-S, Doray B & Kornfeld S Engineering of GlcNAc-1-phosphotransferase for production of highly phosphorylated lysosomal enzymes for enzyme replacement therapy. Mol. Ther. Methods Clin. Dev 5, 59–65 (2017). [PubMed: 28480305]
15. Zhu Y et al. Conjugation of mannose 6-phosphate-containing oligosaccharides to acid α-glucosidase improves the clearance of glycogen in Pompe mice. J. Biol. Chem 279, 50336–50341 (2004). [PubMed: 15383547]
16. Beljaars L et al. Albumin modified with mannose 6-phosphate: a potential carrier for selective delivery of antifibrotic drugs to rat and human hepatic stellate cells. Hepatology 29, 1486–1493 (1999). [PubMed: 10216133]

17. Berkowitz DB, Maiti G, Charette BD, Dreis CD & MacDonald RG Mono- and bivalent ligands bearing mannose 6-phosphate (M6P) surrogates: targeting the M6P/ insulin-like growth factor II receptor. Org. Lett 6, 4921–4924 (2004). [PubMed: 15606100]
18. Das S, Parekh N, Mondal B & Gupta SS Controlled synthesis of end-functionalized mannose-6-phosphate glycopolypeptides for lysosome targeting. ACS **Macro Lett**. 5, 809–813 (2016).
19. Jeanjean A, Garcia M, Leydet A, Montero J-L & Morère A Synthesis and receptor binding affinity of carboxylate analogues of the mannose 6-phosphate recognition marker. Bioorg. Med. Chem 14, 3575–3582 (2006). [PubMed: 16455258]
20. Sly WS et al. Enzyme therapy in mannose receptor-null mucopolysaccharidosis VII mice defines roles for the mannose 6-phosphate and mannose receptors. Proc. Natl Acad. Sci. USA 103, 15172–15177 (2006). [PubMed: 17015822]
21. Kramer JR, Onoa B, Bustamante C & Bertozzi CR Chemically tunable mucin chimeras assembled on living cells. Proc. Natl Acad. Sci. USA 112, 12574–12579 (2015). [PubMed: 26420872]
22. Vidal S, Montero J-L, Leydet A & Morere A A flexible route to mannose 6-phosphonate functionalized derivatives. Phosphorus Sulfur Silicon Relat. Elem 177, 2363–2377 (2002).
23. Jeanjean A et al. Synthesis of new sulfonate and phosphonate derivatives for cation-independent mannose 6-phosphate receptor targeting. Bioorg. Med. Chem. Lett 18, 6240–6243 (2008). [PubMed: 18929485]
24. Ritter TE, Fajardo O, Matsue H, Anderson RG & Lacey SW Folate receptors targeted to clathrin-coated pits cannot regulate vitamin uptake. Proc. Natl Acad. Sci. USA 92, 3824–3828 (1995). [PubMed: 7731991]
25. Johnson DE, Ostrowski P, Jaumouillé V & Grinstein S The position of lysosomes within the cell determines their luminal pH. J. Cell Biol 212, 677–692 (2016). [PubMed: 26975849]
26. Kampmann M, Bassik MC & Weissman JS Functional genomics platform for pooled screening and generation of mammalian genetic interaction maps. Nat. Protocols 9, 1825–1847 (2014). [PubMed: 24992097]
27. Horlbeck MA et al. Compact and highly active next-generation libraries for CRISPR-mediated gene repression and activation. eLife 5, e19760 (2016). [PubMed: 27661255]
28. Heider MR & Munson M Exorcising the exocyst complex. Traffic 13, 898–907 (2012). [PubMed: 22420621]
29. Yamazaki Y, Painter MM, Bu G & Kanekiyo T Apolipoprotein E as a therapeutic target in Alzheimer's disease: a review of basic research and clinical evidence. CNS Drugs 30, 773–789 (2016). [PubMed: 27328687]
30. Li JY et al. A biparatopic HER2-targeting antibody–drug conjugate induces tumor regression in primary models refractory to or ineligible for HER2-targeted therapy. Cancer Cell 29, 117–129 (2016). [PubMed: 26766593]
31. Spangler JB et al. Combination antibody treatment down-regulates epidermal growth factor receptor by inhibiting endosomal recycling. Proc. Natl Acad. Sci. USA 107, 13252–13257 (2010). [PubMed: 20616078]
32. Huang Y et al. Molecular basis for multimerization in the activation of the epidermal growth factor receptor. eLife 5, e14107 (2016). [PubMed: 27017828]
33. Needham SR et al. EGFR oligomerization organizes kinase-active dimers into competent signalling platforms. Nat. Commun 7, 13307 (2016). [PubMed: 27796308]
34. Zhu J, Blenis J & Yuan J Activation of PI3K/Akt and MAPK pathways regulates Myc-mediated transcription by phosphorylating and promoting the degradation of Mad1. Proc. Natl Acad. Sci. USA 105, 6584–6589 (2008). [PubMed: 18451027]
35. Huang P et al. The role of EGF–EGFR signalling pathway in hepatocellular carcinoma inflammatory microenvironment. J. Cell. Mol. Med 18, 218–230 (2014). [PubMed: 24268047]
36. Shen Y et al. Transferrin receptor 1 in cancer: a new sight for cancer therapy. Am. J. Cancer Res 8, 916–931 (2018). [PubMed: 30034931]
37. Weissman AM, Klausner RD, Rao K & Harford JB Exposure of K562 cells to anti-receptor monoclonal antibody OKT9 results in rapid redistribution and enhanced degradation of the transferrin receptor. J. Cell Biol 102, 951–958 (1986). [PubMed: 3005341]

38. Burr ML et al. CMTM6 maintains the expression of PD-L1 and regulates anti-tumour immunity. Nature 549, 101–105 (2017). [PubMed: 28813417]

39. Li W et al. MAGeCK enables robust identification of essential genes from genome-scale CRISPR/Cas9 knockout screens. Genome Biol. 15, 554 (2014). [PubMed: 25476604]

40. Eden E, Navon R, Steinfeld I, Lipson D & Yakhini Z GOrilla: a tool for discovery and visualization of enriched GO terms in ranked gene lists. BMC Bioinformatics 10, 48 (2009). [PubMed: 19192299]

41. Hebert AS et al. Improved precursor characterization for data-dependent mass spectrometry. Anal. Chem 90, 2333–2340 (2018). [PubMed: 29272103]

42. Tyanova S, Temu T & Cox J The MaxQuant computational platform for mass spectrometry-based shotgun proteomics. Nat. Protocols 11, 2301–2319 (2016). [PubMed: 27809316]

43. Cox J et al. Andromeda: a peptide search engine integrated into the MaxQuant environment. J. Proteome Res 10, 1794–1805 (2011). [PubMed: 21254760]

44. Elias JE & Gygi SP Target-decoy search strategy for increased confidence in large-scale protein identifications by mass spectrometry. Nat. Methods 4, 207–214 (2007). [PubMed: 17327847]

45. Cox J et al. Accurate proteome-wide label-free quantification by delayed normalization and maximal peptide ratio extraction, termed MaxLFQ. Mol. Cell. Proteomics MCP 13, 2513–2526 (2014). [PubMed: 24942700]

46. Tyanova S et al. The Perseus computational platform for comprehensive analysis of (prote)omics data. Nat. Methods 13, 731–740 (2016). [PubMed: 27348712]

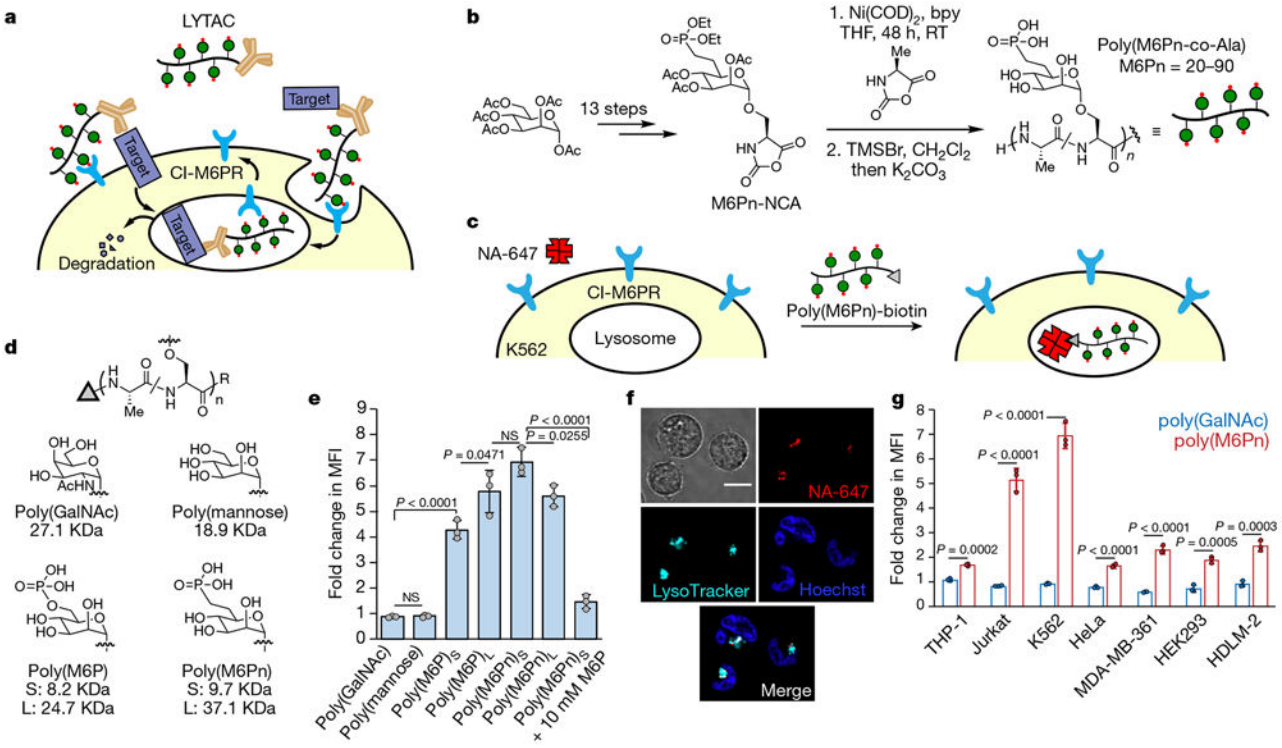

Fig. 1 | LYTACs using CI-M6PR traffic proteins to lysosomes.

a, The concept of LYTACs, in which a glycopolypeptide ligand for CI-M6PR is conjugated to an antibody to traffic secreted and membrane-associated proteins to lysosomes. **b**, Synthesis of M6Pn glycopolypeptide ligands for CI-M6PR. bpy, bipyridyl; COD, cyclooctadiene; RT, room temperature; THF, tetrahydrofuran; TMS, trimethylsilyl. **c**, Assay for the internalization of NA-647 by biotin-based LYTACs. **d**, Panel of synthetic M6P and M6Pn glycopolypeptides and controls. L, long; S, short. **e**, Fold changes in mean fluorescence intensity (MFI) for K562 cells incubated at 37 °C for 1 h with 500 nM NA-647 or 500 nM NA-647 and 2 μM biotinylated glycopolypeptide in complete growth media. MFI was determined by live-cell flow cytometry. **f**, Live-cell confocal microscopy images of K562 cells treated as in **e**, then labelled with LysoTracker Green for 30 min. Scale bar, 10 μm. **g**, Panel of cell lines for NA-647 uptake experiments, performed as in **e**. For **e**, **g**, data are mean ± s.d. of three independent experiments. For **f**, images are representative of two independent experiments. *P* values were determined by unpaired two-tailed *t*-tests; fold changes are reported relative to incubation with protein targets alone. NS, not significant.

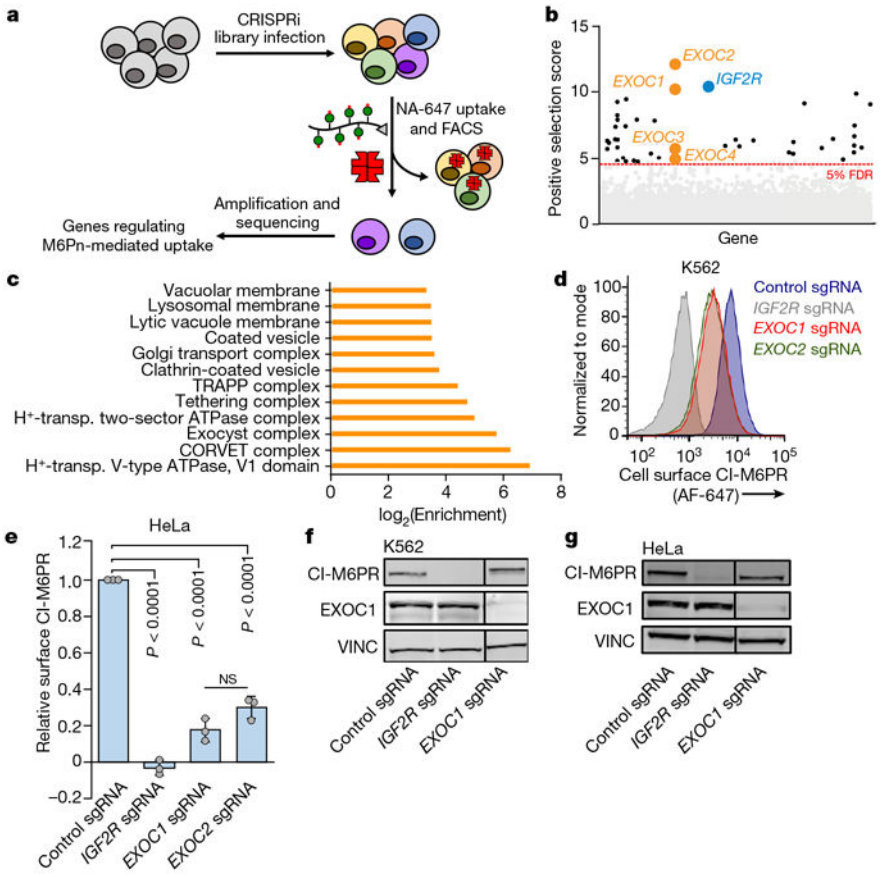

Fig. 2 |. CRISPRi screen identifies key cellular machinery for LYTACs.

a, Schematic of a CRISPRi screen in K562 cells stably expressing dCas9-KRAB and a library of sgRNAs with genome-wide coverage. **b**, Selected gene hits for regulation of NA-647 internalization by LYTACs. **c**, Gene ontology (GO) annotation for significant hits (<5% FDR). **d**, **e**, Cell surface expression levels of CI-M6PR in dCas9-KRAB K562 cells (**d**) or dCas9-KRAB HeLa cells (**e**) transfected with control sgRNA, *IGF2R*-targeting sgRNA, *EXOC1*-targeting sgRNA or *EXOC2*-targeting sgRNA. Cells were stained for CI-M6PR and subjected to live-cell flow cytometry. **f**, **g**, Western blot analysis of EXOC1 and CI-M6PR in K562 (**f**) and HeLa (**g**) CRISPRi knockdown lines. For **c**, analysis is representative of two replicates; **d**, **f**, **g** are representative of two independent experiments. K562 cells rapidly lost the exocyst knockdown phenotype after two passages. For **e**, data are mean ± s.d. of three independent experiments in HeLa and normalized to non-targeting sgRNA. *P* values were determined by unpaired two-tailed *t*-tests.

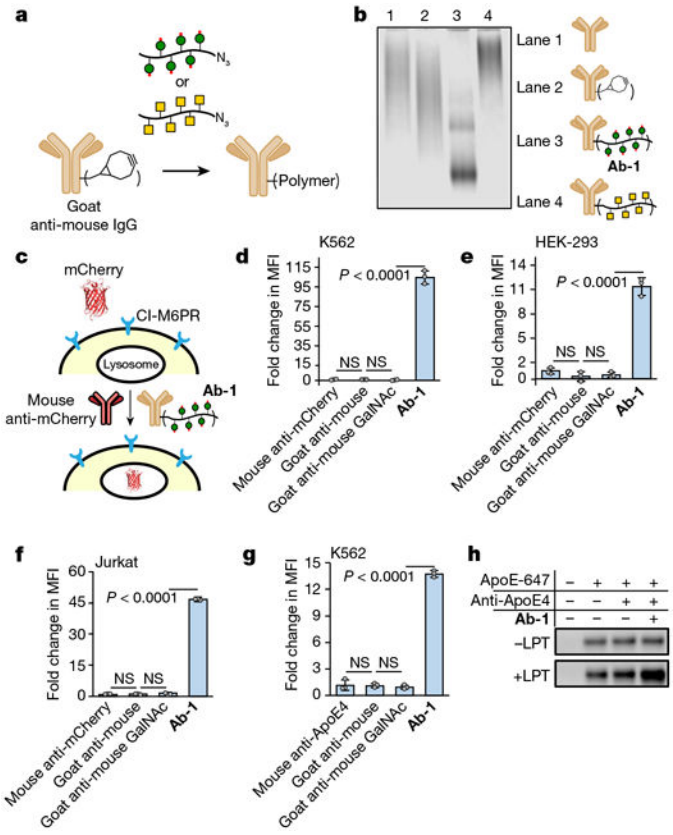

Fig. 3 |. LYTACs target soluble proteins to lysosomes for degradation.

a, Synthetic scheme for antibody-based LYTACs with a goat anti-mouse IgG. **b**, Native gel (with Coomassie staining) of polyclonal goat anti-mouse IgG conjugates. **c**–**f**, Uptake of mCherry antigen and its antibody by a LYTAC, into K562 cells (**d**), HEK-293 cells (**e**) or Jurkat cells (**f**) with 50 nM mCherry, and 25 nM mouse anti-mCherry or 25 nM mouse anti-mCherry with 25 nM goat anti-mouse or conjugates after 1 h at 37 °C. Mean fluorescence intensity (MFI) was measured by live-cell flow cytometry. **g**, Uptake of ApoE4-647 into K562 cells; experiments were performed analogously to **d**. Median fluorescence intensity (MFI) was measured by live-cell flow cytometry. **h**, Cells were incubated as in **g** for 8 h in the presence or absence of 0.1 mg ml^{-1} leupeptin (LPT), then lysed. Lysates were separated by SDS–PAGE, and ApoE4-647 was detected via in-gel fluorescence. Results are representative of two (**h**) or three (**b**) independent experiments. Data are mean ± s.d. of three independent experiments (**d**–**g**). *P* values were determined by unpaired two-tailed *t*-tests.; fold changes are reported relative to incubation with protein targets alone.

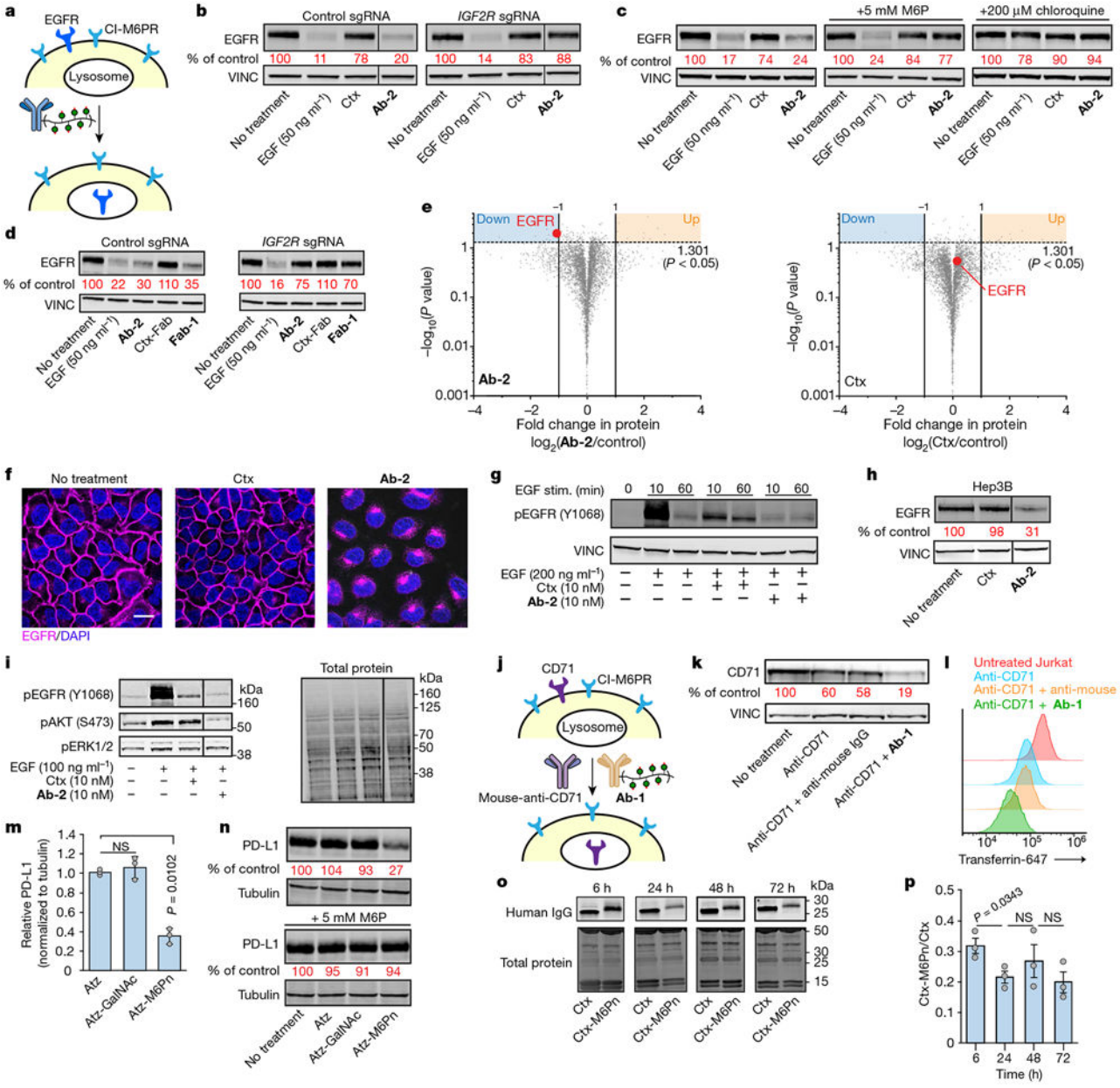

Fig. 4 | LYTACs accelerate degradation of membrane proteins.

a, Schematic of EGFR degradation using LYTACs. **b**, EGFR levels after treatment with 10 nM **Ab-2** for 24 h in dCas9-KRAB HeLa cells expressing a control sgRNA or sgRNA targeting *IGF2R*. **c**, EGFR levels after treatment with 10 nM **Ab-2** for 48 h in dCas9-KRAB HeLa cells expressing a control sgRNA in the presence of 5 mM mannose-6-phosphate (M6P) or 200 μM chloroquine. **d**, EGFR levels after treatment with **Fab-1** in dCas9-KRAB HeLa cells expressing a control sgRNA or sgRNA targeting *IGF2R*. **e**, Fold change in the abundance of 3,877 HeLa proteins detected by quantitative proteomics analysis after 24-h treatment with either 10 nM **Ab-2** (left) or ctx (right) relative to untreated cells, data are the mean of three biological replicates. **f**, Cellular localization of EGFR after treatment with ctx or **Ab-2** for 48 h. Scale bar, 20 μm. **g**, Levels of pEGFR in dCas9-KRAB HeLa cells

expressing a control sgRNA after 24-h incubation with 10 nM ctx or **Ab-2**, then incubation with EGF for 10 min or 60 min. **h**, Levels of EGFR after treatment with 10 nM **Ab-2** in Hep3B cells for 48 h. **i**, Levels of pEGFR, pAkt and pERK1/2 in Hep3B cells after 48 h incubation with 10 nM ctx or **Ab-2**, then incubation with EGF for 30 min. **j**, Degradation of CD71 mediated by a primary antibody and **Ab-1**. **k**, CD71 levels after treatment with 50 nM anti-CD71 or anti-CD71 and **Ab-1** in Jurkat cells after 24 h. **l**, Uptake of transferrin-647 in Jurkat cells treated with anti-CD71 or anti-CD71 and **Ab-1** for 24 h. **m**, PD-L1 levels in HDLM-2 cells after treatment with 25 nM atezolizumab (atz) or atz-LYTAC for 48 h. **n**, Levels of PD-L1 degradation with 25 nM atz-LYTAC after 48 h in HDLM-2 cells in the presence of 5 mM M6P. **o**, Serum levels of ctx or ctx-LYTAC in BALB/c mice injected intraperitoneally at 5 mg kg^{-1}. **p**, Quantification of serum ctx-M6Pn relative to ctx after intraperitoneal injection. Data are representative of two (**c**, **d**, **f**, **g**, **l**, **n**) or three (**b**, **h**, **i**, **k**, **o**) independent experiments or mice (**o**). Data are mean ± s.d. (**m**) or mean ± s.e.m. (**p**) of three independent experiments (**m**, one of which is shown in **n**) or mice (**p**). *P* values were determined by unpaired two-tailed *t*-tests. Relative values were calculated via densitometry and normalized to loading control (**b**–**d**, **h**, **k**, **m**, **n**) or relative to ctx levels (**p**).